AD-A053 858 BROWN UNIV PROVIDENCE R I DEPT OF CHEMISTRY F/G 7/4
THE ELECTRICAL AND OPTICAL PROPERTIES OF THE SYSTEM TIO(2-X)F(X--ETC(U)
UNCLASSIFIED MAY 78 A WOLD N00014-77-C-0387
TR-4 NL

| OF |
AD
A053858

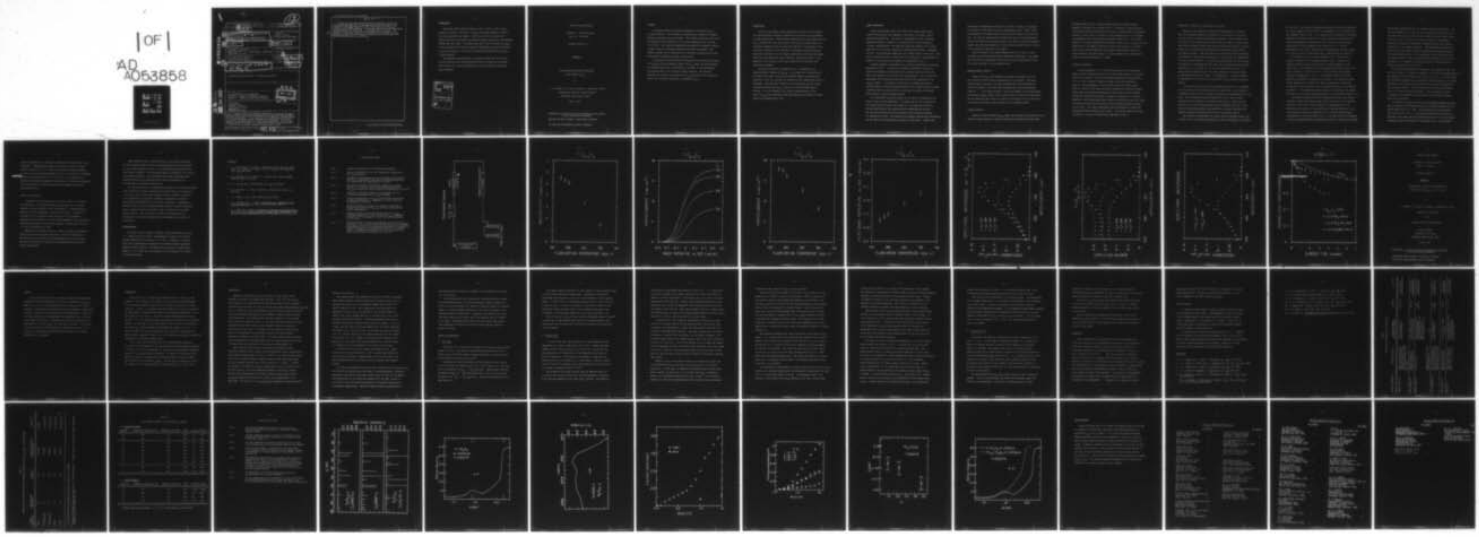

END
DATE FILMED
6 -78
DDC

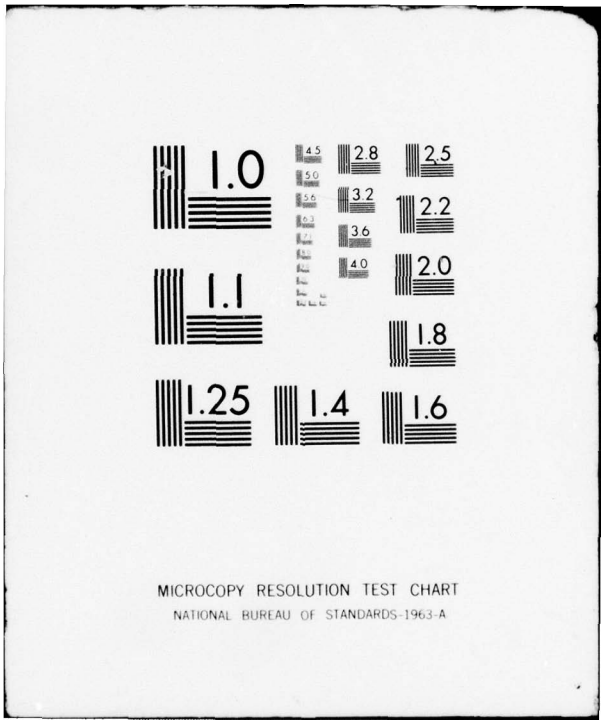
1.0
1.1
1.25
1.4
1.6
1.8
2.0
2.2
2.5
2.8
3.2
3.6
4.0
4.5
5.0
5.6
6.3
7.1
MICROCOPY RESOLUTION TEST CHART
NATIONAL BUREAU OF STANDARDS-1963-A

12

SECURITY CLASSIFICATION OF THIS PAGE (When Data Entered)

REPORT DOCUMENTATION PAGE	READ INSTRUCTIONS BEFORE COMPLETING FORM
1. REPORT NUMBER 4 (14) TR-4	2. GOVT ACCESSION NO. / 3. RECIPIENT'S CATALOG NUMBER
4. TITLE (and Subtitle) (6) THE ELECTRICAL AND OPTICAL PROPERTIES OF THE SYSTEM $TiO_{2-x}F_x$. THE ELECTRICAL, OPTICAL AND PHOTOCONDUCTING PROPERTIES OF $Fe_{2-x}Cr_xO_3$ ($0 \leq x \leq 0.47$).	5. TYPE OF REPORT & PERIOD COVERED Technical 6/1/77 - 5/31/78
	6. PERFORMING ORG. REPORT NUMBER
7. AUTHOR(s) (10) Aaron Wold	8. CONTRACT OR GRANT NUMBER(s) (15) N0014-77-C-0387
9. PERFORMING ORGANIZATION NAME AND ADDRESS Department of Chemistry Brown University INVESTIGATOR: Aaron Wold Providence, RI 02912	10. PROGRAM ELEMENT, PROJECT, TASK AREA & WORK UNIT NUMBERS NR-359-653
11. CONTROLLING OFFICE NAME AND ADDRESS Dr. David Nelson, Code 472 Office of Naval Research Department of the Navy, Arlington, VA 22217	12. REPORT DATE (11) 5/31/78 31 May 78
	13. NUMBER OF PAGES 52
14. MONITORING AGENCY NAME & ADDRESS (if different from Controlling Office) (9) Technical rept. 1 Jun 77- 31 May 78,	15. SECURITY CLASS. (of this report) (12) 51 p.
	15a. DECLASSIFICATION/DOWNGRADING SCHEDULE

16. DISTRIBUTION STATEMENT (of this Report)

Approved for public release; Distribution unlimited

17. DISTRIBUTION STATEMENT (of the abstract entered in Block 20, if different from Report)

18. SUPPLEMENTARY NOTES

Two publications to be submitted:
Section A. Journal of Inorganic Chemistry.
Section B. Journal of Solid State Chemistry.

19. KEY WORDS (Continue on reverse side if necessary and identify by block number)

Photoanodes
Titanium Dioxide
Titanium Oxyfluorides
Iron Oxide
Chromium Iron Oxide

20. ABSTRACT (Continue on reverse side if necessary and identify by block number)

A convenient method for preparing compounds in the system $TiO_{2-x}F_x$ is described and the photoelectrolytic behavior of TiO_{2-x} and $TiO_{2-x}F_x$ anodes has been investigated. It was found that the substitution of small amounts of fluorine for oxygen in TiO_2 increases the photocurrent output which arises from increased response at the longer wavelengths. The improved response may be attributed to the increase in depletion layer width which is supported by an observed increase in resistivity. (cont)

DD FORM 1 JAN 73 1473 EDITION OF 1 NOV 65 IS OBSOLETE S/N 0102-014-6601

405 436

SECURITY CLASSIFICATION OF THIS PAGE (When Data Entered)

$0 < x \leq 0.47$

A study has also been carried out on the electrical, optical and photoconducting properties of pure and reduced single crystals of the composition $Fe_{2-x}Cr_xO_3$ where $0 \leq 0.47$. It has been found that pure α-Fe_2O_3 is not a photoconductor. A necessary condition for the observation of photocurrents in n-type Fe_2O_3 is that some Fe_3O_4 be present. In addition, it has been found that the substitution of chromium for iron in α-Fe_2O_3 results in a montonically decreasing optical band gap as the chromium concentrations, x, increases.

alpha

INTRODUCTION

During the current year from June 1st, 1977 to May 31, 1978, we have studied two systems. The first is $TiO_{2-x}F_x$ where small amounts of fluorine have been substituted for oxygen. It will be seen from the report that follows that small substitutions of fluorine markedly increase the photocurrents obtained for TiO_2 anodes. The second study deals with the systems $Fe_{2-x}Cr_xO_3$. It will be shown that in order to obtain a photocurrent from Fe_2O_3 electrodes, Fe_3O_4 must be present. The effect of substituting chromium into $Fe_{2-x}Cr_xO_3$ is also discussed.

The following technical report is therefore divided into two sections. The first dealing with improved substituted fluorine anodes and the second section deals with a careful examination of Fe_2O_3 and chromium substituted Fe_2O_3 electrodes.

OFFICE OF NAVAL RESEARCH

Contract No. N00014-77-C-0387

Task No. NR-359-653

TECHNICAL REPORT NO. 4

SECTION A

THE ELECTRICAL AND OPTICAL PROPERTIES OF THE SYSTEM $TiO_{2-x}F_x$

by

S. N. Subbarao, Y. H. Yun, R. Kershaw, K. Dwight and A. Wold*

Department of Chemistry, Brown University

Providence, Rhode Island 02912

May 31, 1978

*To whom all correspondence should be addressed.

ABSTRACT

A convenient method for preparing compounds in the system $TiO_{2-x}F_x$ has been developed. The electronic and photoelectric properties of samples prepared accordingly have been studied. The fluorine content was found to be an essentially linear function of the reaction temperature over the range 575 to 700°C. The saturation photocurrent increased with decreasing fluorine content, because of increased response at the longer wavelengths. This improved response may be attributed to the increase in depletion-layer width arising from the observed increase in resistivity.

A significantly larger saturation photocurrent was obtained from samples of $TiO_{2-x}F_x$ than from comparable samples of TiO_{2-x} under the same conditions. The increased output may be attributed to a decrease in the recombination rate brought about by the filling of oxygen vacancies. The long-term stability was studied, and a sample of $TiO_{2-x}F_x$ was found to be at least as stable, in a suitable electrolyte, as comparable TiO_{2-x}.

INTRODUCTION

In most of the previous studies dealing with oxides which have served as n-type electrodes, increased conductivity was achieved by the production of oxygen deficiencies. Whereas earlier publications on n-type anodes such as TiO_{2-x} indicated that they were stable, there has been recent evidence (1) that these compounds do not show long term stability in the presence of the production of oxygen at their surfaces. An alternate method of producing conducting electrodes is by the chemical substitution of fluorine for oxygen, rather than the creation of oxygen vacancies. Both methods result in the formation of $3d^1$ titanium, which would account for the relatively high conductivity obtained.

In a recent publication, Derrington, et al. (2) reported on the photoelectrolytic behavior of $WO_{3-x}F_x$. It was found that the substitution of fluorine for oxygen in WO_3 did not adversely affect the photoelectric properties of WO_3, but increased the stability of the compound when used as a photoanode. One might expect members of the system $TiO_{2-x}F_x$ also to show increased stability over TiO_{2-x}, since all of the anion sites would be occupied. It is the purpose of this study to prepare members of the series $TiO_{2-x}F_x$ and to determine their photocurrents and stability as photoanodes in photoelectrolysis cells.

SAMPLE PREPARATION

Wafers one millimeter thick were sliced from a single crystal boule obtained from National Lead Industries, South Amboy, New Jersey, using a water-cooled diamond saw. Each wafer was sandblasted in order to produce homogeneous surfaces, cleaned in an ultrasonic bath, and then wrapped in a piece of platinum gauze. The gauze and wafer were inserted into a sleeve made from 0.005 inch thick titanium foil obtained from MRC Corp., Orangeburg, New York. The encapsulated sample was then centered within a nickel boat. This boat was positioned within a nickel tube (the "sample"tube) and centered with respect to the hot zone of one furnace, as illustrated in Fig. 1.

Hydrogen fluoride was generated by the thermal decomposition of potassium bifluoride at 260°C. A nickel boat containing approximately 18 grams of potassium bifluoride was positioned within a second nickel tube (the "KHF_2" tube), and centered in the hot zone of a second furnace. Fig. 1 depicts the arrangement of the furnaces and gas train used for the preparation of the $TiO_{2-x}F_x$ samples. A gas mixture of 85% argon 15% hydrogen was dried by passing through a phosphorus pentoxide drying tube, flowed over the potassium bifluoride (which was kept at 260°C), passed over the sample, and finally exited through a sodium hydroxide bubbler.

The fluorinating system was purged with 85% argon 15% hydrogen gas for about 12 hours at room temperature. The sample tube was then positioned in its furnace and both furnaces were turned on. The sample was allowed to heat and equilibrate at the desired reaction temperature for one hour. The KHF_2 tube was then placed in its furnace, which already had reached the temperature of 260°C. The generation of hydrogen fluoride began immediately, and the time of the fluorination run started at that moment. Samples were

fluorinated at temperatures between 575°C and 700°C. Attempts to fluorinate a TiO_2 wafer at 550°C failed to yield a homogeneous product. After 8 hours of fluorination, the sample furnace was shut off and allowed to cool for one hour. The tube was removed from the furnace and cooled to room temperature. The exit gas stream was then tested with pH test paper to verify that hydrogen fluoride was still being produced. The KHF_2 tube was removed from its furnace and the sample was taken out of its sleeve.

Samples prepared in this manner appeared pale blue to black in color. The darker colors resulted from higher temperature preparations. Each sample was subdivided into appropriate pieces for the ensuing measurements by means of a string saw using a silicon carbide slurry.

THERMOGRAVIMETRIC ANALYSIS

Samples of $TiO_{2-x}F_x$ were prepared for analysis by grinding a piece of each fluorinated wafer to give approximately 100 mg of sample. The finely divided powder was heated in an oxygen atmosphere from room temperature to 1000°C and changes in the weight were recorded using a Cahn electrobalance (Model RG) and a chart recorder. None of the samples in the series showed any measurable weight change, which indicated that the fluorine had substituted for the oxygen and that, within the limits of the analysis ($\sim$0.01), there were no measurable additional vacancies present in the compounds studied.

FLUORINE ANALYSIS

Samples of finely divided $TiO_{2-x}F_x$ powder were subjected to pyrosulfate fusion. During the fusion process, a stream of nitrogen gas saturated with water vapor

was passed over the melt. The gas stream carried the hydrogen fluoride produced by hydrolysis of the sample into a 1 M solution of sodium hydroxide. The resulting solution was diluted to 50 ml with a buffer solution of potassium acetate and acetic acid. The final pH of the solution was 5.5. The fluoride was determined with an Orion fluoride electrode (Model 94-09). The fluoride content of the sample fluorinated at 700°C gave a value of x in $TiO_{2-x}F_x$ of 0.002, whereas that of the sample fluorinated at 600°C gave a value of x = 0.0001, which was the limit detectable by the fluoride electrode and is subject to some uncertainty, since the value of x in this material can be reported only within an accuracy equivalent to $\pm$ 0.0002.

ELECTRICAL PROPERTIES

A bar approximately 4 x 2 x 1 mm was cut from each of the fluorinated wafers in such a fashion that only the two large faces belonged to the outside surface of the sample. Each bar was further subdivided into three sections 4 x 2 x 0.25 mm in order to establish whether or not each fluorinated wafer was truly homogeneous. Thus the middle section was taken entirely from the interior of the wafer and made no contact with the outside surface. Indium leads were bonded ultrasonically to each section, and the standard Van der Pauw technique (3) was used to measure its resistivity. Excellent agreement, within experimental error, between the resistivity values for inside and outside sections was obtained for all the fluorinated wafers considered in this study. This result demonstrates that the fluorination process had penetrated uniformly throughout each sample. The measured resistivity values are shown as a function of fluorination temperature in Fig. 2.

PHOTOELECTRIC PROPERTIES OF FLUORINATED TiO_2 ANODES

Electrodes were prepared by cutting pieces approximately 4 mm square from the fluorinated samples and evaporating a thin coating of copper onto the back of each to provide good electrical contacts. Anode assemblies were fabricated by using indium metal to solder these electrodes to platinum wires which had been sealed in small pyrex tubes, and then coating all but the front surface with an electrically insulating resin (Microstop, Michigan Chrome and Chemical Company). Care was taken not to disturb the active photosurface. For measurement, these anodes were mounted in a small glass cell approximately 8 mm from the quartz window. A platinized platinum cathode (2.5 cm^2 in area) was mounted 2 cm behind and below the anode, and a saturated calomel reference electrode (SCE) 10 cm above it. The cell was filled with 100 ml of 0.2 M sodium acetate electrolyte (pH $\cong$ 7.5) which was purged of dissolved oxygen by continuous bubbling of 85% argon - 15% hydrogen gas. A cathode potential of approximately -0.64 volts vs. SCE was used as the criterion for completed purging.

A 150 watt xenon arc was used to illuminate an aperture 5 mm in diameter, which was imaged onto the anode by means of a quartz lens. This resulted in a reproducible area 2.25 mm in diameter irradiated with approximately 50 mw total power. The instantaneous power was determined for each curve by using a calibrated Eppley thermopile (16-junction Coblentz-type). Anodic bias was applied via a voltage follower having an output impedance less than 0.1 ohm, and the resulting photoresponse was measured with a current amplifier which inserted a megligible potential drop (<1μv) in the external circuit.

The variation of photocurrent with anode potential (measured against SCE) is shown in Fig. 3 for samples fluorinated at several temperatures (T_F) between

575 and 700°C. The indicated photocurrent densities have all been normalized to a total irradiation of 12.5 mw/mm^2, corresponding to 50 mw incident over the illuminated area of 4 mm^2. It is evident that the saturation photocurrent (measured at an anode potential of 0.6 volts) increases significantly with decreasing fluorination temperature over this range, and the essentially linear nature of this relationship can be seen in Fig. 4. The peak photocurrent of 17.9 ma/cm^2 obtained here is approximately twice the maximum (9.2 ma/cm^2) found with unfluorinated TiO_{2-x} under similar conditions (4).

The lateral shift of the curves presented in Fig. 3 results from a systematic variation of the flat-band potential (U_{fb}). Values for U_{fb} (measured against SCE) were obtained from the linear dependence of the square root of the photocurrent upon anode potential for small values of the current (values <0.5 ma/cm^2 in Fig. 3). They are shown plotted against fluorination temperature in Fig. 5. The observed increase in flat-band potential corresponds to a decrease in its energy. This decrease in energy appears anomalous for an increase in carrier concentration, which would be expected to raise the Fermi level, but similar behavior has been reported elsewhere (5). The determining factor may well be a lowering of the valence band because of the greater electronegativity of the substituted fluorine (6,7).

The spectral photoresponse of the fluorinated electrodes was studied by inserting an Oriel monochrometer (Model 7240) in place of the 5 mm aperture. The curves shown in Fig. 6 were obtained at an anode potential of 0.6 volts with a slit width of 0.5 mm, which gave a spectral resolution of 4 nm. The photocurrents have been normalized so as to yield integrated outputs corresponding to the values given in Fig. 4. This data can also be expressed in terms of quantum efficiency (electrons per photon) by dividing the observed

photocurrent (electrons/sec) by the incident radiation (photons/sec). The curves presented in Fig. 7 have not been corrected for any absorption in the electrolyte or cell window, nor for reflection from the sample surface. From Figs. 6 and 7, it can be seen that the increase in photocurrent observed with decreasing fluorination temperature arises from increased responsivity at the longer wavelengths. These wavelengths penetrate more deeply into the electrodes, and their photogenerated electron-hole pairs will become separated only if this penetration is less than the width of the depletion layer. Thus the improved response observed at low T_F may be attributed to the increase in depletion-layer width resulting from the increase in resistivity seen in Fig. 2.

The spectral photoresponse of a sample of TiO_{2-x} reduced at 600°C has also been measured. The results, normalized to 9.2 ma/cm^2 integrated output, (4) are compared with those obtained for $TiO_{2-x}F_x$ in Fig. 8. It is evident that the fluorinated material gives an appreciably greater response at the longer wavelengths, which effect can be attributed to an absence of vacancies in the fluorinated samples. The solar spectrum falls off much more rapidly below 400 nm than the xenon-arc spectrum. Thus the disparity between the outputs of fluorinated and reduced rutile would be greatly enhanced under solar irradiation.

In addition, the long-term stability of electrodes prepared from these same two samples has been determined under 12.5 mw/mm^2 irradiation with an applied anodic bias of 1.5 volts. The resulting decay of photocurrent with time is shown in Fig. 9. The fluorinated electrode was found to be appreciably less stable than the reduced electrode in 0.2 M sodium acetate, presumably because of hydrolysis of the fluorine ions. Such hydrolysis

should be surpressed by a sufficient concentration of fluoride ions in the electrolyte. Measurements were made in a lucite cell having a fluorite window 2 mm thick with a 0.2 M solution of potassium bifluoride buffered to a pH of 6 with potassium hydroxide and with a 0.2 M solution of unbuffered potassium bifluoride (pH=3.5). As seen in Fig. 9, the hydrolysis was partially and completely surpressed, respectively, by these two electrolytes. In the latter case, the long-term stability was improved over that of unfluorinated rutile.

SUMMARY AND CONCLUSIONS

A procedure for the fluorination of 1 mm thick wafers of rutile has been developed. The resulting products $TiO_{2-x}F_x$ were found to contain fluorine by chemical analysis, to be stoichiometric by thermogravimetric analysis, and to be homogeneous by resistivity analysis. The value of x was found to be an essentially linear function of the fluorination temperature over the range 575 to 700°C from measurements of the resistivity, saturation photocurrent, and flat band potential. Analysis gave the value $x = 0.002$ for preparation at 700°C.

Samples with the smallest value of x showed the largest photocurrent, despite their having the highest resistance. Most of the variation of photocurrent with x occurred in the long-wavelength part of the spectrum, and hence was attributed to variation of the depletion-layer width with carrier concentration.

Under irradiation from a xenon are source, rutile wafers fluorinated at 575°C produced almost twice the photocurrent obtained from rutile reduced at the optimum temperature (600°C). The long-wavelength photoresponse was significantly enhanced in the fluorinated material, presumable by the filling of the oxygen vacancies. This enhancement would become appreciably more pronounced under solar irradiation, which provides considerably less relative power at wavelengths below 350 nm.

The long-term stability of fluorinated electrodes in a suitable electrolyte under conditions of intense irradiation and extreme anodic bias was found to be at least as good as that of an optimally reduced electrode. Hydrolysis of the electrodes was completely surpressed by maintaining an adequate concentration of fluoride ions in the aqueous electrolyte. Furthermore, it should be noted that the fluorinated material produced a higher photocurrent than the reduced electrode even after 4 hours of operation in the sodium acetate solution. Thus it appears that definite improvement over the photoelectric efficiency of reduced rutile electrodes can be achieved by fluorination.

ACKNOWLEDGEMENT

The office of Naval Research, Arlington, Virginia supported the work of S. N. Subbarao and Kirby Dwight. Acknowledgement is made to the National Science Foundation for the support of Y. H. Yun. In addition, the authors would like to acknowledge the support of the Materials Research Laboratory Program at Brown University. The authors would also wish to express their support to Dr. W. Godek for his assistance with the development of a method for fluorine analysis.

REFERENCES

1. L. A. Harris and R. H. Wilson, J. Electrochem. Soc., 123, 1010 (1976) Also, L. A. Harris, D. R. Cross, and M. E. Gerstner, J. Electrochem. Soc., 124, 839 (1977).

2. C. E. Derrington, W. S. Godek, C. A. Castro, and A. Wold, Inorganic Chemistry, 17, 977 (1978).

3. L. J. Van der Pauw, Phillips Tech. Rev., 20, 220 (1958).

4. S. N. Subbarao, Y. H. Yun, R. Kershaw, K. Dwight and A. Wold, to be published.

5. J. F. Dewald, J. Phys. Chem. Solids, 14, 155 (1960).

6. J. O. McCaldin and T. C. McGill, Electrochem. Soc. Monograph on Thin Films and Interfaces, ed. Mayer, et al. in press, (1977).

7. W. P. Gomes and F. Cardon, Proceedings of Conference on Electrochemistry and Physics of Semiconductor-Liquid Interfaces Under Illumination, Airlie VA, ed. A. Heller, Electrochemical Soc., Princeton, N.J., p. 120 (1977).

FIGURE CAPTION SHEET

FIG. 1 - Schematic illustration of the fluorination apparatus.

FIG. 2 - Variation of resistivity with the fluorination temperature of $TiO_{2-x}F_x$ electrodes.

FIG. 3 - Dependence of photocurrent upon anode potential (SCE reference) for $TiO_{2-x}F_x$ electrodes fluorinated at various temperatures T_F for "white" xenon arc irradiation of 1.25 w/cm^2.

FIG. 4 - Variation of saturation photocurrent, measured at an anode potential of 0.6 volts, with the fluorination temperature of $TiO_{2-x}F_x$ electrodes for "white" xenon arc irradiation of 1.25 w/cm^2.

FIG. 5 - Variation of flat-band potential (SCE reference) with the fluorination temperature of $TiO_{2-x}F_x$ electrodes.

FIG. 6 - Spectral photoresponse of $TiO_{2-x}F_x$ for electrodes fluorinated at various temperatures T_F, normalized to "white" xenon arc irradiation of 1.25 w/cm^2.

FIG. 7 - Quantum efficiency in electrons per photon as a function of excitation wavelength for $TiO_{2-x}F_x$ electrodes fluorinated at various temperatures T_F.

FIG. 8 - Comparison between the spectral photoresponse of $TiO_{2-x}F_x$ electrodes fluorinated at 575°C and that of TiO_{2-x} electrodes reduced at 600°C, normalized to "white" xenon arc irradiation of 1.25 w/cm^2.

FIG. 9 - Comparison between the decay of photocurrent with time for TiO_{2-x} electrodes in 0.2 M sodium acetate and that for $TiO_{2-x}F_x$ electrodes fluorinated at 575°C in 0.2 M potassium bifluoride, 0.2 M potassium bifluoride buffered with potassium hydroxide, and 0.2 M sodium acetate. Measurements were made with 1.5 volts of anodic bias under "white" xenon arc irradiation of 1.25 w/cm^2.

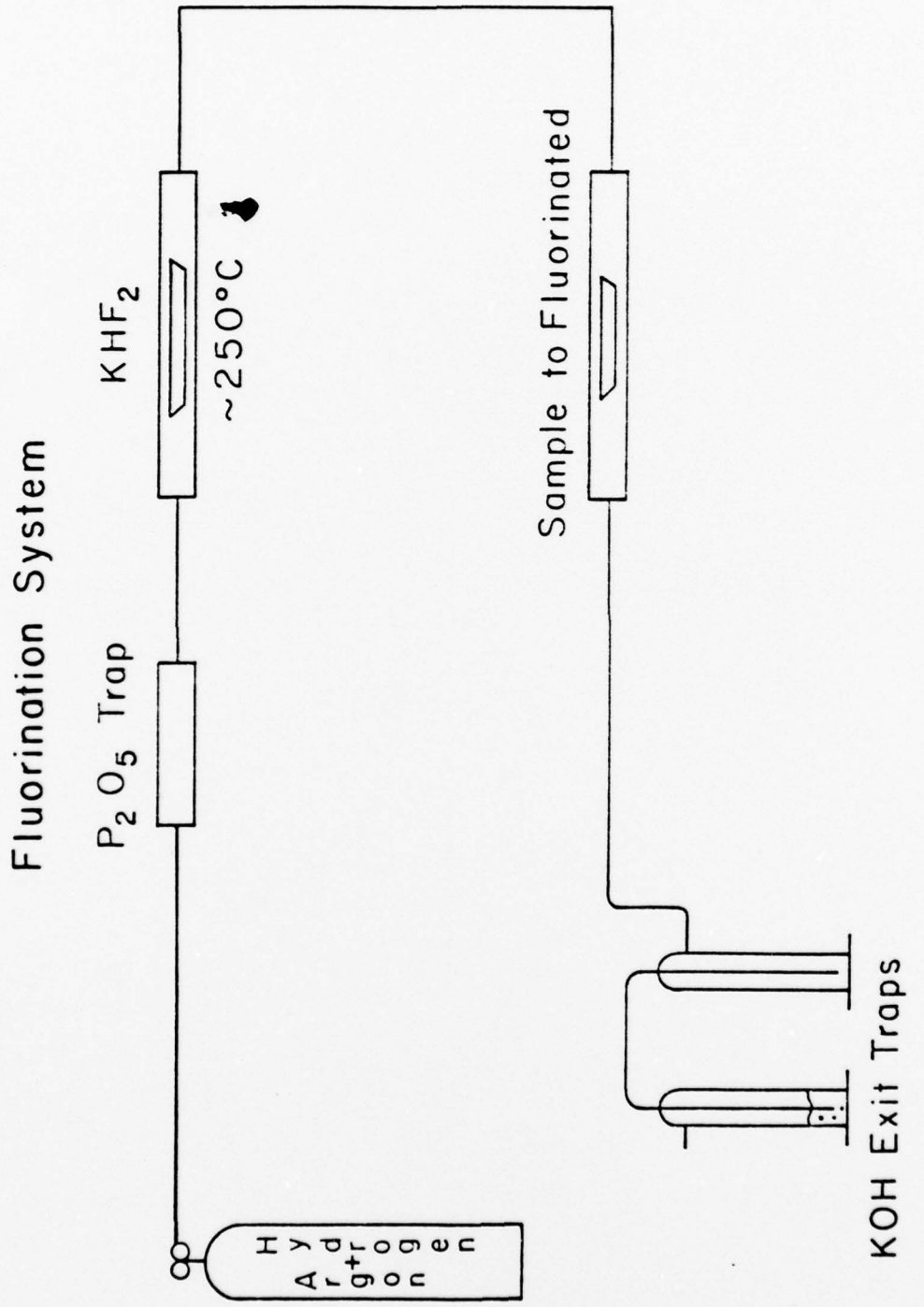
Fluorination System
P_2O_5 Trap
KHF_2
~250°C
Sample to Fluorinated
Hydrogen
KOH Exit Traps

Fig 1

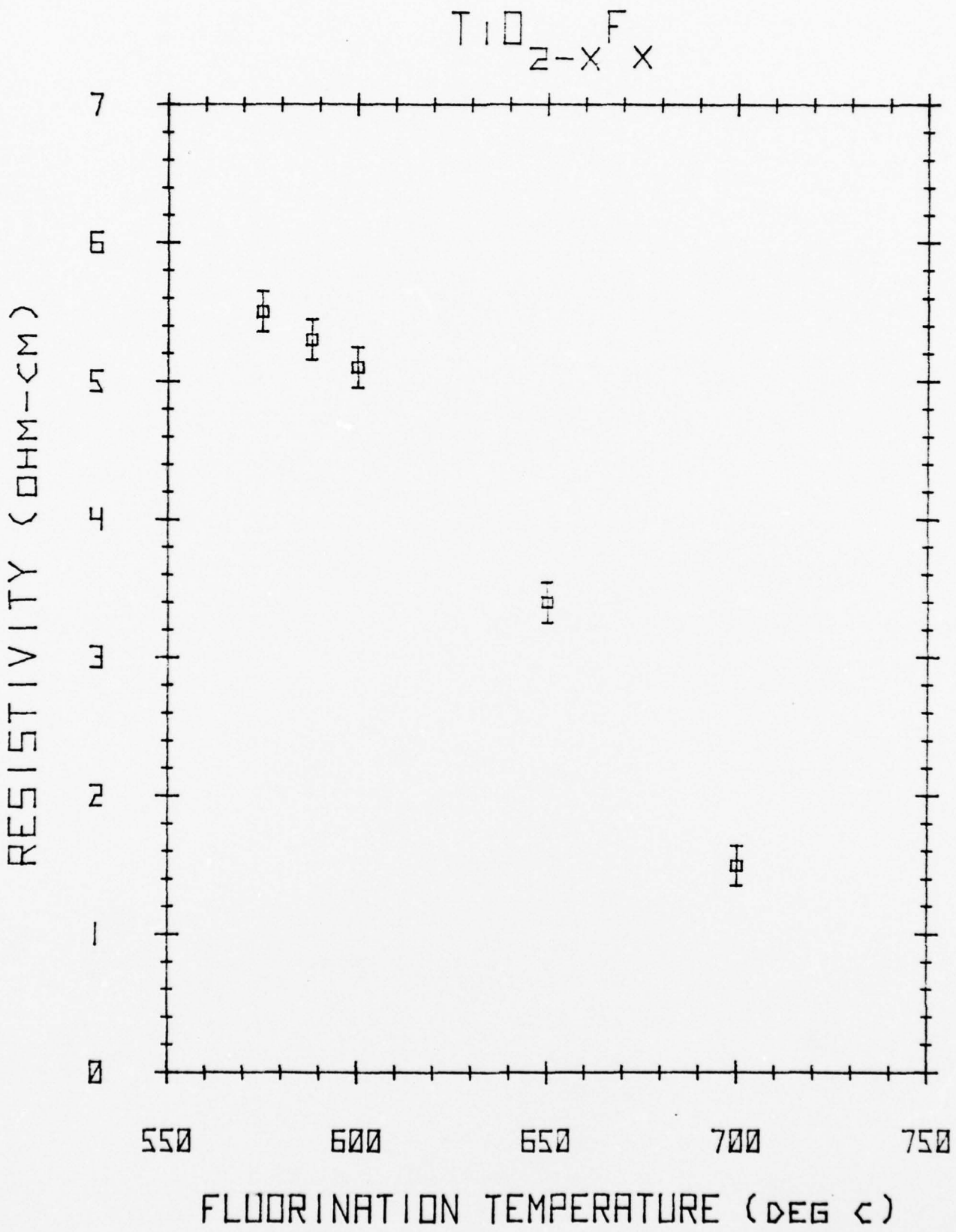
$TiO_{2-x}F_x$
RESISTIVITY (OHM-CM)
0
1
2
3
4
5
6
7
550
600
650
700
750
FLUORINATION TEMPERATURE (DEG C)

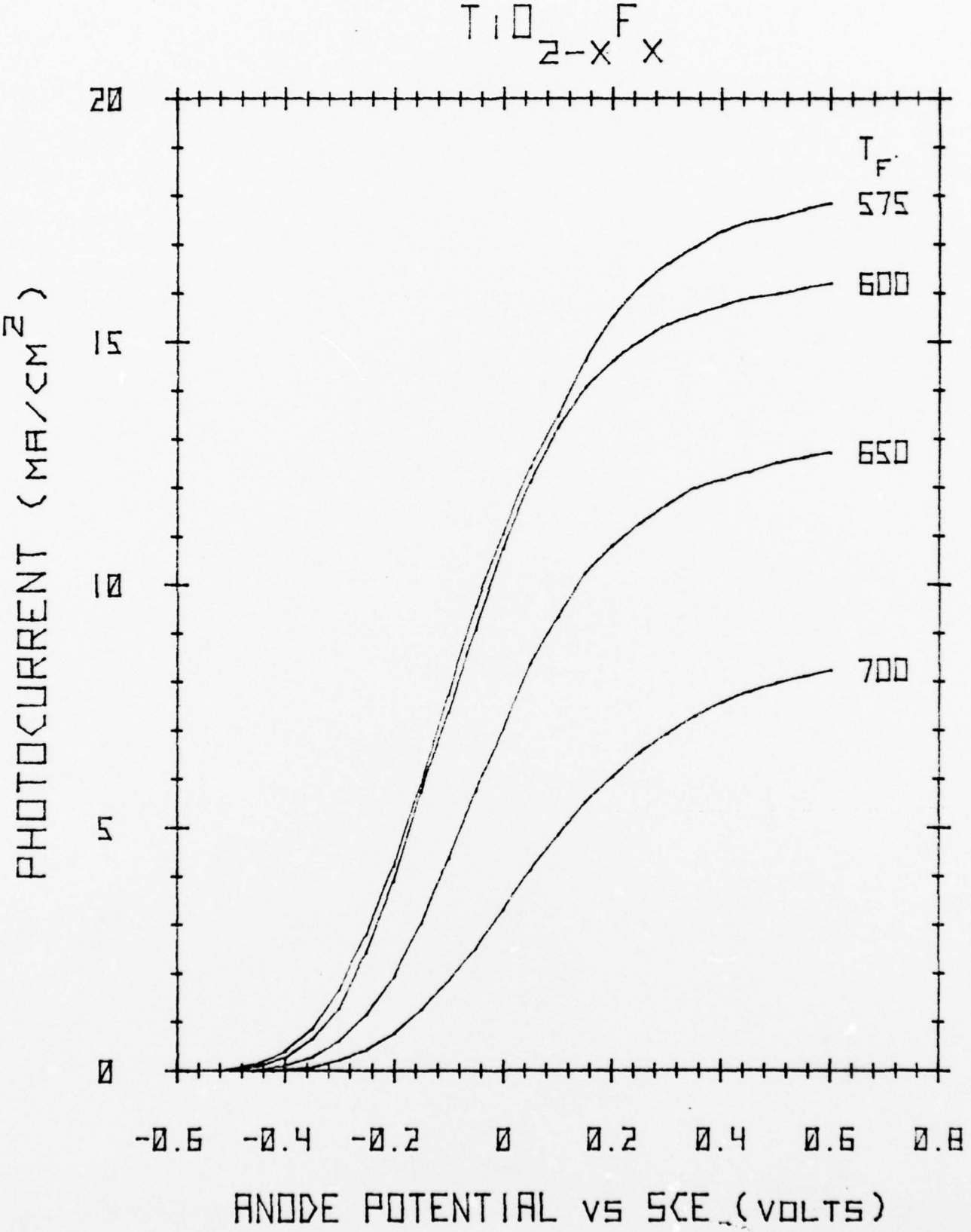
$TiO_{2-x}F_x$
20
15
10
5
0
T_F
575
600
650
700
PHOTOCURRENT (MA/CM^2)
-0.6
-0.4
-0.2
0
0.2
0.4
0.6
0.8
ANODE POTENTIAL vs SCE (VOLTS)

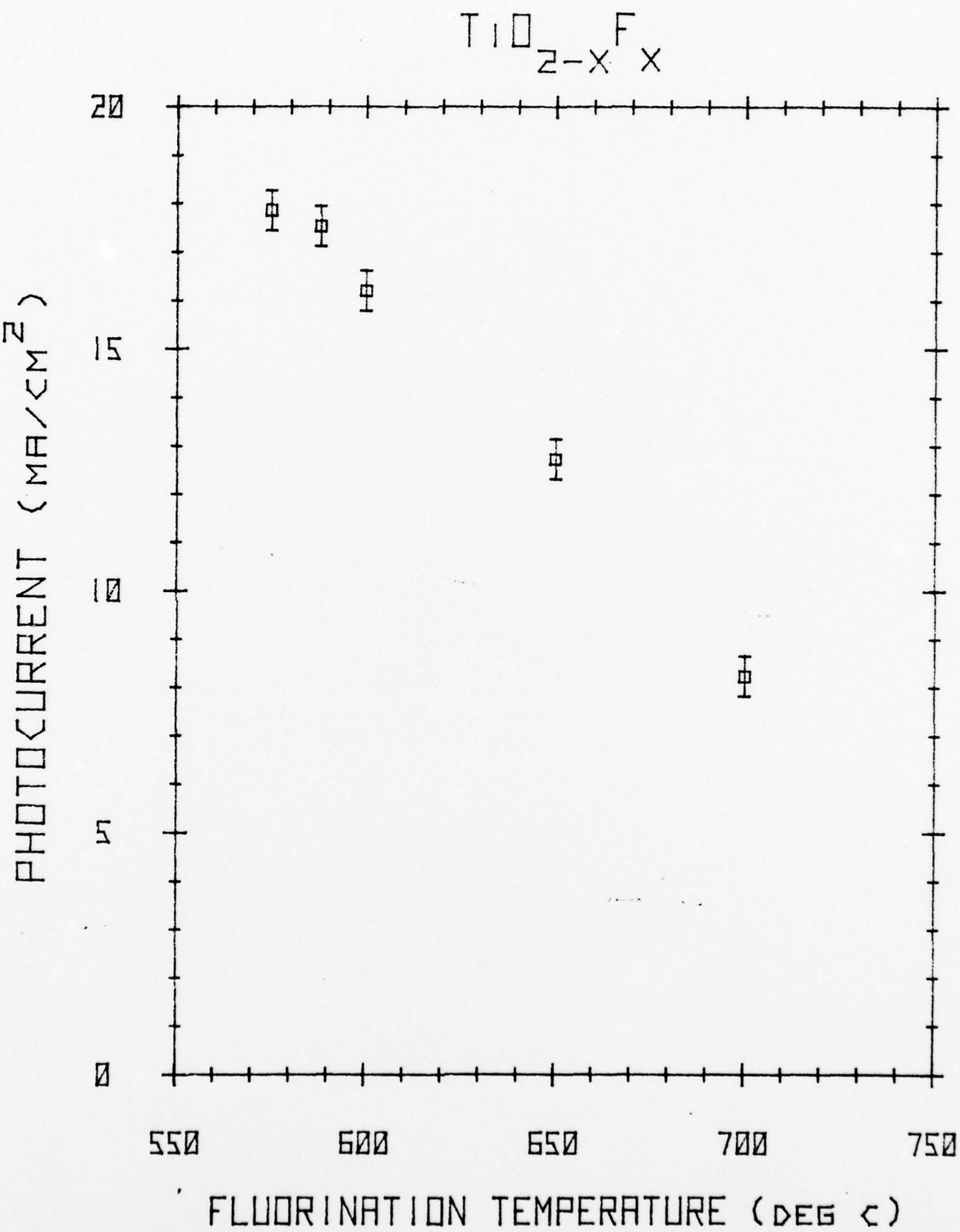
$TiO_{2-x}F_x$
20
15
10
5
0
PHOTOCURRENT (MA/CM^2)
550
600
650
700
750
FLUORINATION TEMPERATURE (DEG C)

Fig 4

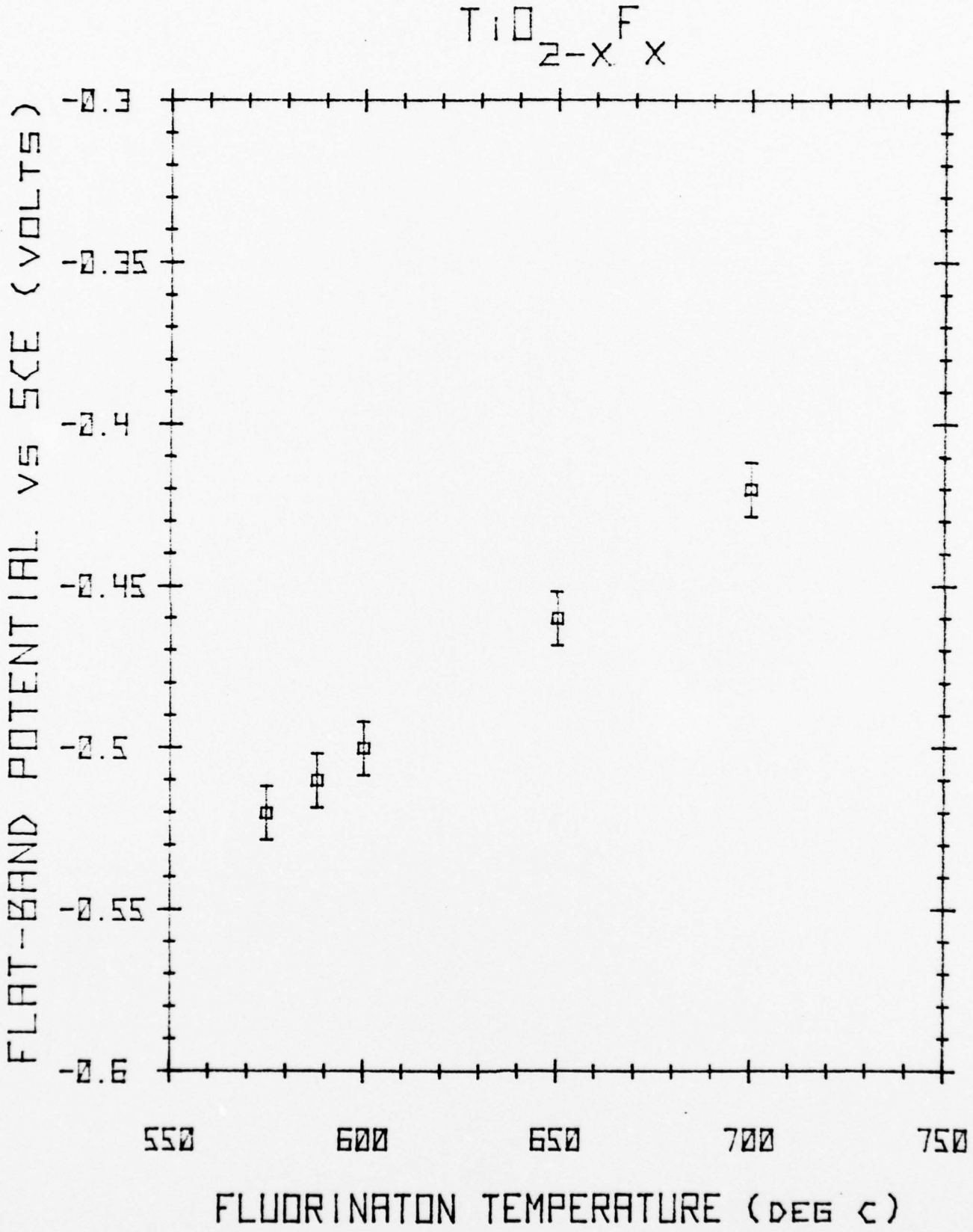
TiO2-xFx
FLAT-BAND POTENTIAL VS SCE (VOLTS)
-0.3
-0.35
-0.4
-0.45
-0.5
-0.55
-0.6
550
600
650
700
750
FLUORINATON TEMPERATURE (DEG C)

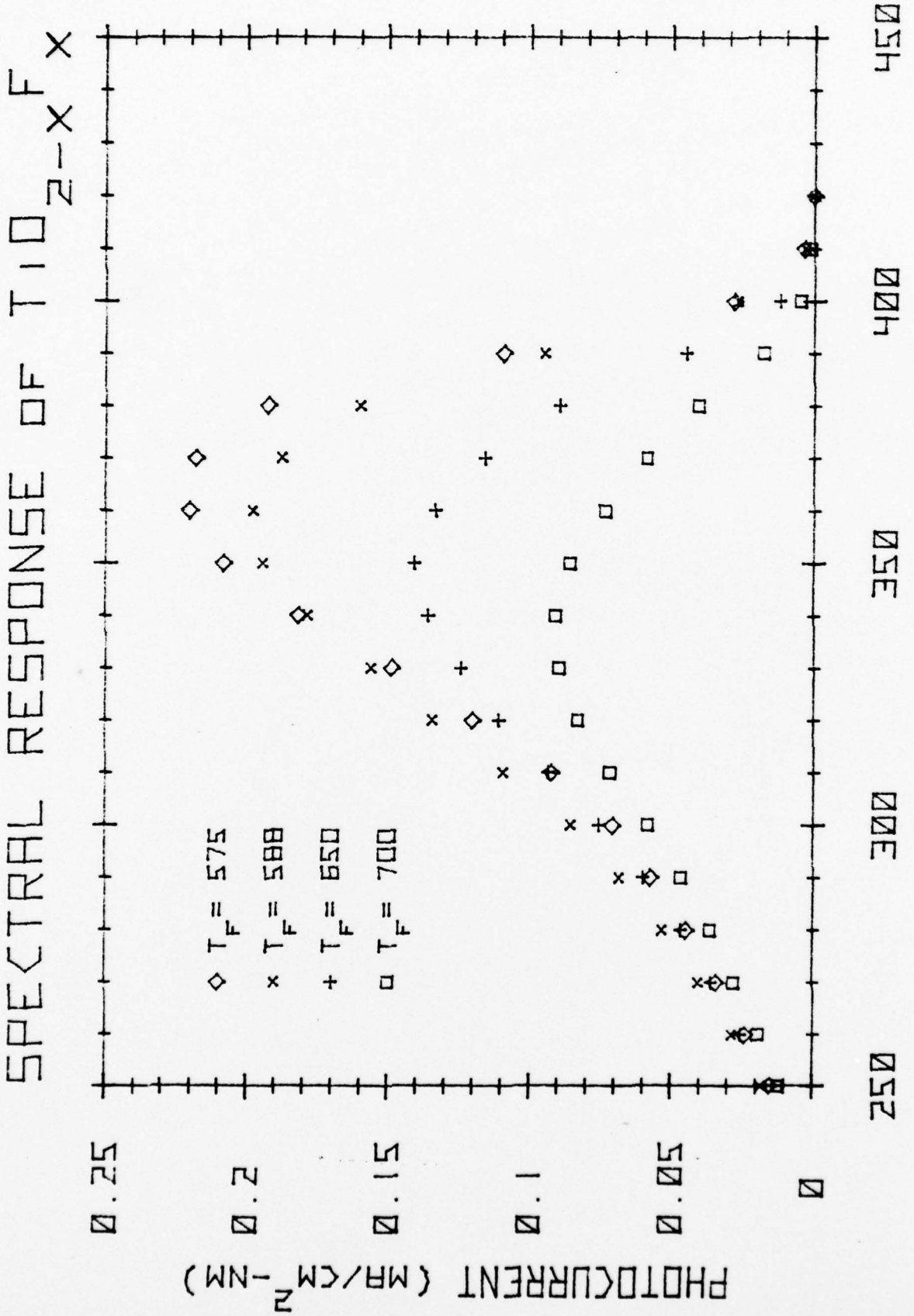
SPECTRAL RESPONSE OF TiO2-XF
PHOTOCURRENT (MA/CM2-NM)
WAVELENGTH (NM)
0
0.05
0.1
0.15
0.2
0.25
250
300
350
400
450
TF = 575
TF = 588
TF = 650
TF = 700

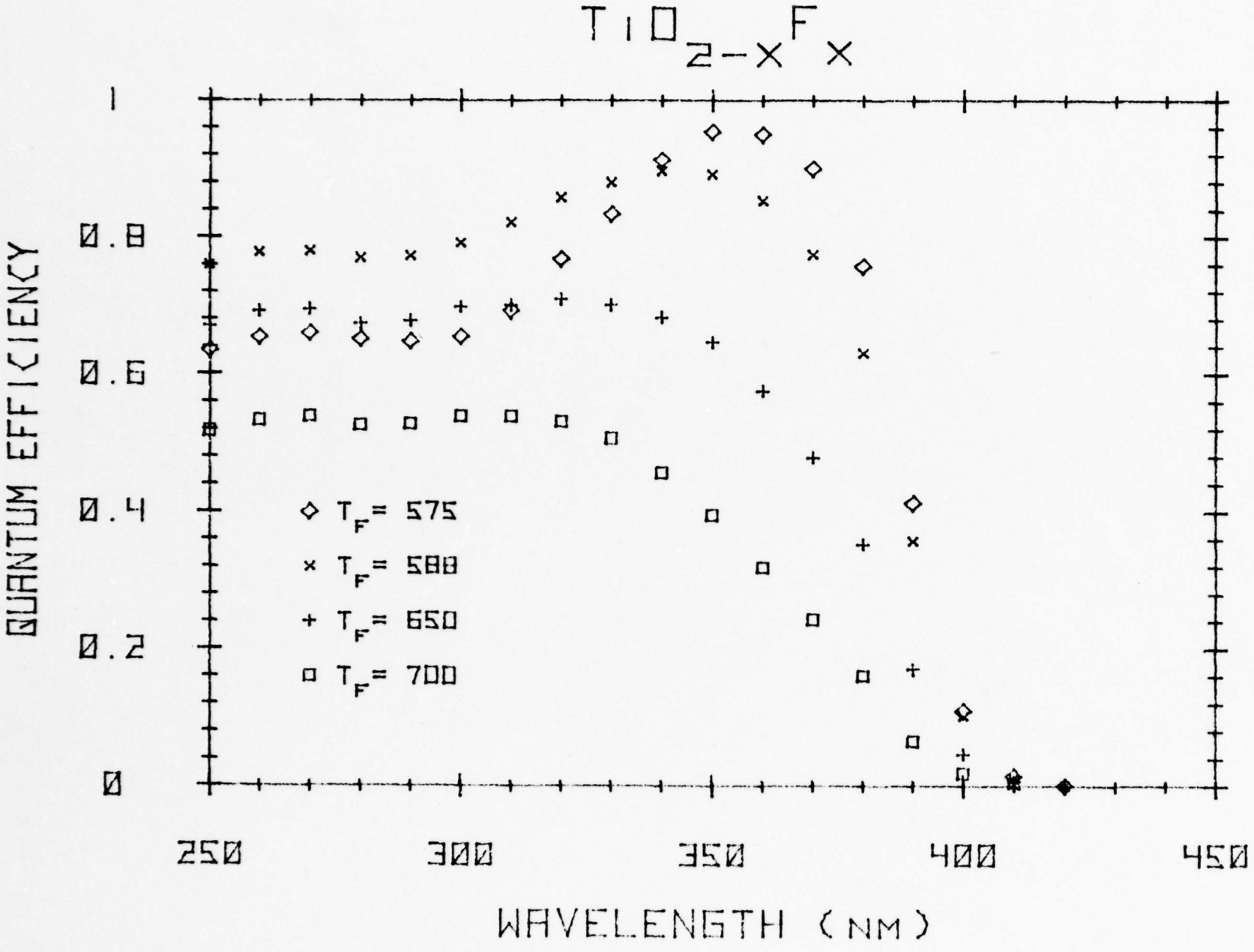
$TiO_{2-x}F_x$
QUANTUM EFFICIENCY
1
0.8
0.6
0.4
0.2
0
250
300
350
400
450
WAVELENGTH (NM)
T_F= 575
T_F= 588
T_F= 650
T_F= 700

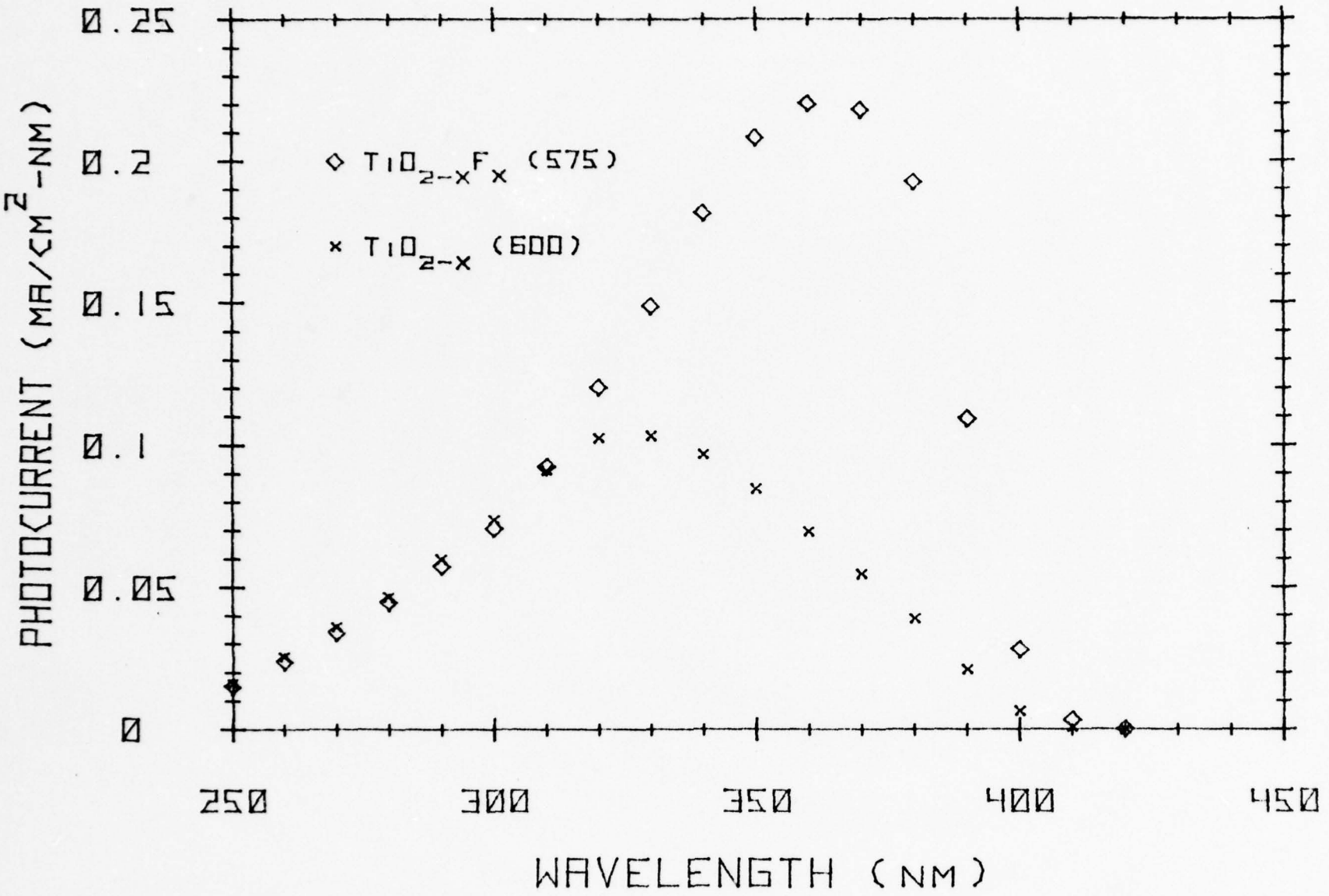
SPECTRAL RESPONSE
0.25
0.2
0.15
0.1
0.05
0
PHOTOCURRENT (MA/CM^2-NM)
◇ $TiO_{2-x}F_x$ (575)
× TiO_{2-x} (600)
250
300
350
400
450
WAVELENGTH (NM)

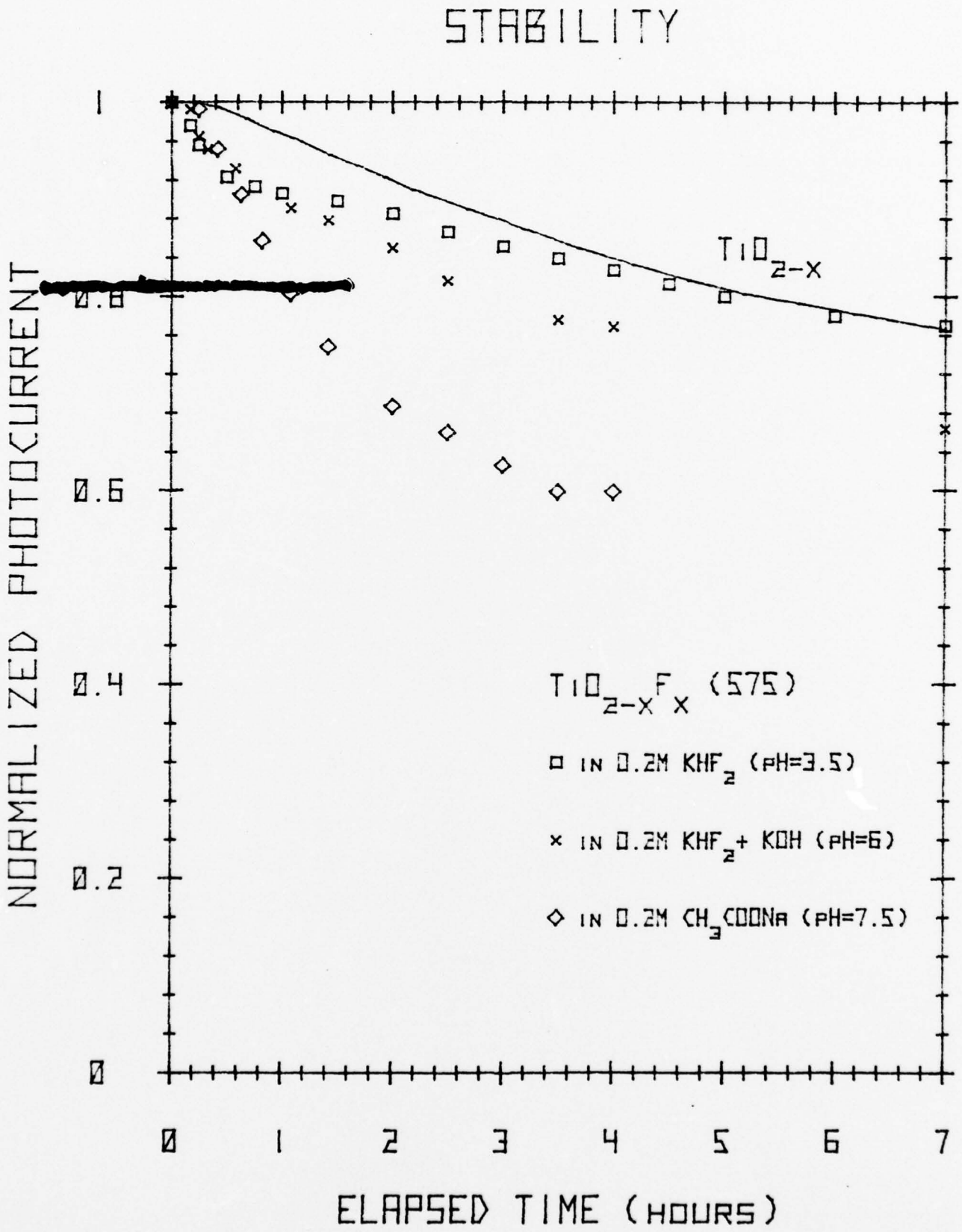
STABILITY
NORMALIZED PHOTOCURRENT
1
0.8
0.6
0.4
0.2
0
0
1
2
3
4
5
6
7
ELAPSED TIME (HOURS)
TiO2-X
TiO2-XFX (575)
□ IN 0.2M KHF2 (pH=3.5)
× IN 0.2M KHF2+ KOH (pH=6)
◇ IN 0.2M CH3COONa (pH=7.5)

OFFICE OF NAVAL RESEARCH

Contract No. N00014-77-C-0387

Task No. NR-359-653

TECHNICAL REPORT NO. 4

SECTION B

THE ELECTRICAL, OPTICAL AND PHOTOCONDUCTING PROPERTIES OF $Fe_{2-x}Cr_xO_3$ ($0 \leq x \leq 0.047$)

by

P. Merchant, R. Collins, R. Kershaw, K. Dwight and A. Wold*

Prepared for Publication

in the

Journal of Solid State Chemistry

Brown University

Department of Chemistry

Providence, Rhode Island 02912

May 31, 1978

*To whom all correspondence should be addressed.

ABSTRACT

A study has been made of the electrical, optical and photoconducting properties of pure and reduced single crystals of composition $Fe_{2-x}Cr_xO_3$ where $0 \leq x \leq 0.47$. It has been found that pure α-Fe_2O_3 is not a photoconductor. When defect free crystals of α-Fe_2O_3 are reduced a surface layer of Fe_3O_4 is formed and the crystals exhibit photoconductivity. Removal of this layer resulted in the disappearance of photocurrents and an increase in the sample resistivity. A necessary condition for the observation of photocurrents in n-type Fe_2O_3 is that some Fe_3O_4 be present. In addition, it has been found that the substitution of chromium for iron in α-Fe_2O_3 results in a monotonically decreasing optical band gap as the chromium concentration, x, increases.

INTRODUCTION

Several reports (1-5) describing photoconductivity in n-type Fe_2O_3 have appeared in the literature. The interest in this material has been generated by its relatively narrow band gap (2.2 eV) (1-5) and its stability in aqueous solutions. However, it is apparent from these reports (1-5) that the composition of these samples, and therefore the origin of the observed photocurrents, is not well understood (see Table I). Even for the cases where analyses have been reported (2,3), some questions remain concerning the composition of the products studied. In particular, the low resistivities listed in Table I are typical of the impure Fe_2O_3 samples previously characterized by Gardner, et al. (6). It will be evident below that x-ray analysis, which was used to characterize the various products reported in Table I, is not as sensitive a technique as resistivity measurements in determining sample purity.

In this study, the electrical, optical and photoconducting properties of α-Fe_2O_3 have been measured on both pure and slightly reduced samples containing $< 1\%$ Fe_3O_4. From these measurements the origins of the photocurrents previously reported in Fe_2O_3 samples can be determined. In addition, an investigation has been made to study the lowering of the optical band gap of α-Fe_2O_3 by making solid solutions of the system $Fe_{2-x}Cr_xO_3$. Since Cr_2O_3 has a band gap of 1.68 eV (7), members of this system should have band gaps between 1.68 eV and 2.2 eV.

EXPERIMENTAL

Members of the system $Fe_{2-x}Cr_xO_3$ were grown as large single crystal platelets (2-100 mm^2) by chemical vapor transport. Iron (III) oxide (Mapico Red), chromium (III) oxide (Jarrell-Ash) and approximately 20 mg of elemental tellurium were placed into 11 mm ID, 15 cm long silica tubes and evacuated to less than 2μ Hg. Chlorine gas was then introduced to give a partial pressure of 380 torr. The tubes were sealed and transport was attempted at several charge and growth zone temperatures. The conditions for successful transport, and the analyses of the products are given in Table II. The tubes were first heated in the back-transport mode for over 18 hrs. and then transport allowed to proceed for periods longer than 5 days. The samples were then removed from the tubes and washed in 3M hydrochloric acid followed by rinsing with dilute ammonium hydroxide and finally by distilled water. The larger crystals showed a uniform blue-grey appearance by reflected light while the thinnest platelets were found to transmit red light, indicative of a band gap of approximately 2 eV.

Some of the pure Fe_2O_3 crystals were ground into powders and their composition analyzed using a Norelco x-ray diffractometer having a monochromatic, high intensity copper source [λ ($CuK\alpha_1$) = 1.5405 Å]. Slow scan patterns having silicon as an internal standard showed that these crystals were single phase α-Fe_2O_3 (corrundum structure) with lattice constants a = 5.033Å, c = 13.755Å. No evidence of the presence of Fe_3O_4 or other phases of Fe_2O_3 was found in any of these crystals. Laue back-reflection photographs, taken with a General Electric XRD-3 diffractometer unit having a tungsten source showed that the $Fe_{2-x}Cr_xO_3$ platelets were oriented with their c-axes perpendicular to the large faces. The values of x in $Fe_{2-x}Cr_xO_3$ were determined by neutron activation

analysis (see Table II).

The reduced samples were prepared by placing the crystals in evacuated silica tubes containing titanium turnings (not in direct contact with the crystals) and heating them to temperatures ranging from 350-425°C for periods exceeding 150 hrs. These temperatures were determined by the appearance of Fe_3O_4 in the x-ray patterns of the products obtained by reducing pure α-Fe_2O_3 powders (see Fig. 1) for more than 12 hrs. at 50°C intervals ranging from 150-600°C. Resistance measurements were used to determine the reduction times for single crystals as follows. One of the α-Fe_2O_3 crystals, having a resistance greater than $10^8\Omega$ before reduction, was reduced at 375° for 193 hrs. and its resistance was found to decrease to 6.6 kΩ. Further reduction of this sample for another 127 hrs lowered the resistance to 2.2 kΩ. Because of the small relative change in the resistance of this sample for the second reduction, 150 hours was chosen as a minimum time for the reduction of the crystals of this study.

The resistivities (ρ) of the samples were measured in the c-plane using the Van der Pauw technique (8). Ohmic contacts were obtained by the ultrasonic soldering of indium directly to the platelet edges. Hall effect measurements were not attempted since the samples showed magnetic behavior.

The optical measurements were taken at room temperature with unpolarized light in the 2100-270 nm region using a Cary Model 17 spectrophotometer. Absorbance measurements were made with the light incident along the c-axis of the samples. The reflectivities of the samples were measured with the light incident at a 20° angle to the c-axis and ratioed against the calibrated reflectance of an evaporated aluminum film. None of the samples required polishing since

the washed crystals had surfaces comparable to those obtained by polishing to a 0.05μ finish.

The photoelectrolysis cell consisted of a platinized platinum cathode and semiconducting anode in a 0.2M sodium acetate solution through which a 15% H_2, 85% Ar gas mixture was bubbled to purge the solution of dissolved oxygen. This gave a cathode potential of -0.65 volts with respect to the saturated calomel electrode (SCE). Illumination was provided by an Oriel 150W xenon lamp which was focused into a 2 mm diameter spot (12.5 mW/mm^2) an the anode. Measurements of the light and dark currents were taken at room temperature as a function of the bias voltage applied between the anode and cathode.

RESULTS AND DISCUSSION

a) Pure Fe_2O_3

From Table I it is seen that the resistivity of the pure α-Fe_2O_3 samples exceeds 10^6 Ω-cm. Such values of resistivity are characteristic of high purity α-Fe_2O_3 (6) (which exhibits intrinsic conductivity, since all of the iron present has the high spin state $3d^5$.)

Measurements of the optical density of thin platelets of pure α-Fe_2O_3 show the existence of a direct gap at 2.16 ± 0.03 eV (see Fig. 2). This peak has been assigned to the $^6A_{1g} \rightarrow {}^4E_g\ (t_{2g})^3\ (e_g)^2$ crystal field transition by Tandon and Gupta (9). The lower energy peak at 1.44 ± 0.03 eV has been assigned to the $^6A_{1g} \rightarrow {}^4T_{1g}\ (t_{2g})^4\ (e_g)$ crystal field transition by the same authors (9).

The large absorption coefficient of these samples for photon energies above 2.3 eV precluded transmission measurements. Consequently, reflectivity measurements were necessary to study the optical properties in this spectral region. In the UV there is a reflectance minimum at 3.64 $\pm$ 0.04 eV (341 nm), as shown in Fig. 3. It may be of interest to note that the energy of this reflectance minimum coincides roughly with the energy of the peak in the photocurrent vs photon energy curves for n-type Fe_2O_3 electrodes (1-3).

None of the pure α-Fe_2O_3 crystals showed any detectable change ($\gtrsim 5\mu A/cm^2$) in their light vs dark currents when placed in the photoelectrolysis cell. These results are consistent with the high purity and hence high resistivity of these crystals.

b) Reduced Fe_2O_3

It is well known that Fe_3O_4 (magnetite) is a good conductor at room temperature (10), having a band gap of 0.11 eV (11). Although the phase boundary between α-Fe_2O_3 and Fe_3O_4 is very sharp (12), α-Fe_2O_3 might be made conducting by the introduction of small amounts of Fe_3O_4 into the crystal by reduction. In this process, the removal of oxygen from the structure results in the separation of a spinel phase. Magnetite contains both Fe^{3+} and Fe^{2+} on octahedral sites, hence conduction can then occur via the transfer of electrons from Fe^{2+} to Fe^{3+}.

Upon removal of the reduced crystals from the reduction tubes, it was noticed that they had a blue-black, tarnished appearance in contrast to the blue-grey appearance of the pure α-Fe_2O_3 crystals. The results of

the resistivity measurements are presented in Table III-a. It is interesting to note the constancy of the surface resistance (ρ/d) values with respect to reduction time and temperatures. In particular, all of the samples of group 3 were reduced in the same tube. Although their thicknesses and resistivities varied over about an order of magnitude, their surface resistances vary from one another by less than 20%. These results suggest that only a surface layer of conducting Fe_3O_4 is formed on the samples during reduction and hence that the resistivity of the bulk can be shorted by the surface layer.

A confirmation of this hypothesis was obtained by sanding the surfaces of four of the reduced samples and then measuring their resistivities again. The sanding was accomplished by rubbing both faces and the outer edge with a dilute 600 grit emery paper for about 1 min under a pressure of a few ounces. The changes in thickness (d), resistivity (ρ), and surface resistance (ρ/d) of these samples, caused by the sanding process, can be seen from a comparison of Tables III-a and III-b. One of these samples, #1c, was sanded more heavily with 2/0 emery paper for about 2 min before being rubbed with the 600 grit paper. In this case, there was a nearly complete removal of the Fe_3O_4 layer as seen from its ρ and ρ/d values as well as from its return to a blue-grey appearance after sanding.

Samples 1A and 1B, which were not sanded, were ground into powders and x-ray diffractometer slow scans made for the appearance of the strongest Fe_3O_4 peaks. In both cases, no evidence of detectable amounts of Fe_3O_4 were found. However, as seen in Fig. 1, it is known that Fe_3O_4 is produced by reduction at temperatures greater than or equal to 350°C. It is therefore apparent that resistivity measurements are more sensitive than x-ray analysis

in detecting small amounts of Fe_3O_4 in α-Fe_2O_3 crystals.

The optical densities of three of the reduced α-Fe_2O_3 samples were also measured in the 2100-550 nm region of the spectrum. While the positions of the absorption bands of these samples were identical to those found in the pure Fe_2O_3 samples, it was found that the overall absorbance in the measured spectral region had increased by a constant amount. Since the band gap of Fe_3O_4 occurs below the long-wavelength edge of the spectral region covered by these measurements, a surface layer of Fe_3O_4 should therefore contribute to an additional absorbance in these samples. The constancy of this extra absorbance is consistent with the fact that these measurements were taken at energies above the band gap of Fe_3O_4, where its absorption coefficient is nearly constant (11).

Photocurrent measurements were taken from several of the reduced α-Fe_2O_3 samples. Fig. 4 shows a plot of the light and dark currents of one of these samples (#1c from Table III-b, reduced at 350°C for 163 hrs) as a function of the applied bias. Of interest is the lack of saturation of the photocurrent for the larger bias voltages. This effect was also seen in the other samples of this study as well as in the CVD films of Hardee and Bard (1,3). After removal from the photoelectrolysis cell, this sample was sanded with 2/0 emery paper and its photocurrent measured again. No detectable photocurrents were found after this treatment.

The observation of photocurrents in reduced α-Fe_2O_3, but not in pure α-Fe_2O_3, implies that a necessary condition for the observation of photocurrents in Fe_2O_3 is that it contain mixed valency iron ions. An unfortunate aspect of the reduction of pure, defect free α-Fe_2O_3 crystals is that only a surface layer

of Fe_3O_4 could be formed. As a result, the photocurrents of these samples are limited by the recombination of holes, migrating toward the anode-electrolyte interface, with mobile electrons in the conducting surface layer. Attempts to convert a large part of the pure Fe_2O_3 crystals to Fe_3O_4 resulted in the collapse of the crystal structure. This is due to the inability of the corundum structure to tolerate large concentrations of spinel inclusions.

However, some of the α-Fe_2O_3 crystals were found to have terraced faces, indicative of uneven growth rates in different regions of the crystals. It is well known that in such crystals there exist dislocation networks forming grain boundaries (13). A reduction of these defect crystals might result in the formation of Fe_3O_4 along dislocations where the structure can accommodate spinel inclusions more readily than in more perfect regions of the crystal, thus providing a more uniform mixture of Fe_2O_3 and Fe_3O_4 than in the reduced, defect free platelets.

The results of several photocurrent measurements on one of the reduced defect crystals are presented in Fig. 5. The data for curve 1 was taken when this sample was first placed in the photoelectrolysis cell. Upon removal from the cell, its surface was lightly sanded with 2/0 emery paper for about 2 min followed by a similar abrasion with dilute 600 grit emery paper. It was then replaced in the cell and the points of curve 2 measured. Further repetition of the sanding process resulted in the curves labeled 3 and 4, respectively. It is evident from these plots that there is a large increase in the photocurrent as the conducting surface layer of Fe_3O_4 is removed. As seen from the insert of Fig. 5, the removal of the surface layer is coupled with an increase in the photocurrent to dark current ratio (I_ℓ / I_d). Further sanding of this sample did not result in any significant

changes from the results of curve 4. It is therefore apparent that curve 4 is indicative of the photoconducting behavior of the bulk of this sample.

These results can be interpreted in the following manner. The photocurrents of the unsanded sample (curve 1) are limited by recombination in the conducting Fe_3O_4 surface layer. This view is supported by the relatively large dark currents of this sample before sanding. As the conducting surface layer is removed, the dark currents decrease and the photocurrent increases because of the more homogenous distribution of Fe_3O_4 in α-Fe_2O_3 below the surface. When the surface layer is completely removed, as for curve 4, the true photoconductivity of the bulk is evident.

c) $Fe_{2-x}Cr_xO_3$, $x \neq 0$

The effect of Cr doping on the band gap of α-Fe_2O_3 is presented in Fig. 6 for $0 \leq x \leq 0.47$. For the range of compositions studied, it is apparent that there is a monotonic decrease in the gap of this material as the chromium content, x, increases. The nature of this shift of the energy gap with chromium content can be clarified with a comparison of the optical densities of pure and chromium-doped Fe_2O_3, shown in Fig. 7. It is apparent that the 1.44 eV transition in α-Fe_2O_3 has been shifted to higher energies, whereas the band gap transition is shifted to lower energies, consistent with a reduction in the crystal field splitting of the t_{2g} - e_g levels when chromium is substituted for iron in these samples.

The resistivities of the $Fe_{2-x}Cr_xO_3$ samples listed in Table II were also measured. For all of these samples, the resistivities remained larger than 10^6 Ω-cm at room temperature. This result is interesting since, in these

crystals, the chromium ions are stable in the +3 valence state, $3d^6$. Although the impurity concentration is large, the crystals are not conducting since the iron is still present in only the +3 valence state.

Some of the $Fe_{2-x}Cr_xO_3$ crystals were reduced under conditions similar to those used to reduce the pure α-Fe_2O_3 samples. However, the reduced products possessed no mechanical strength, and fell apart during attempts to attach leads.

Finally, photocurrent measurements were attempted on some of the unreduced $Fe_{2-x}Cr_xO_3$ samples. The lack of mixed valency iron and hence the high resistivity of these samples resulted in no detectable photocurrents in any of these samples.

CONCLUSIONS

Several conclusions may be drawn from the results presented above. First, pure α-Fe_2O_3 is not a photoconductor because of its high resistivity which results from the presence of iron in only a single valence state. A necessary condition for the observation of photocurrents in α-Fe_2O_3 is that it contain Fe^{2+} and Fe^{3+}. When pure, defect free crystals of α-Fe_2O_3 are reduced, only a surface layer of conducting Fe_3O_4 is formed. While this surface layer is responsible for photoconductivity in these crystals, its removal results in a disappearance of the photocurrents in these samples. When crystals containing dislocations are reduced, Fe_3O_4 can form both on the surface and along the dislocations. In this case, the photocurrents increase when the surface layer is removed since this layer reduces the photocurrents by recombination. Therefore, it is desirable to have a

homogeneous mixture of Fe^{2+} and Fe^{3+} present in the crystals to minimize recombination losses. Finally, one can lower the band gap of α-Fe_2O_3 by the formation of the solid solution $Fe_{2-x}Cr_xO_3$.

ACKNOWLEDGEMENTS

The Office of Naval Research, Arlington, Virginia supported the work of Paul Merchant and Kirby Dwight. Acknowledgement is made to the Donors of the Petroleum Research Fund, administered by the American Chemical Society, Washington, D. C. for support of R. Collins. In addition, the authors would like to acknowledge the support of the Materials Research Laboratory Program at Brown University.

The authors wish to express their appreciation to Dr. S. N. Subbarao for his assistance in the study of photocurrents, to Dr. M. Doyle of the State of Rhode Island Nuclear Reactor Facility for assistance in all aspects of the neutron activation analysis, and Professor C. Elbaum of the Brown University Physics Department for several helpful discussions.

REFERENCES

1. K. L. Hardee and A. J. Bard, J. Electrochem. Soc., 123, 1024 (1976).
2. R. K. Quinn, R. D. Nasby and R. J. Baughman, Mat. Res. Bull., 11, 1011 (1976).
3. K. L. Hardee and A. J. Bard, J. Electrochem. Soc., 124, 215 (1977).
4. L. R. Yeh and N. Hackerman, J. Electrochem. Soc., 124, 833 (1977).
5. H. H. Kung, H. S. Jarrett, A. W. Sleight and A. Ferretti, J. Appl. Phys., 48, 2463 (1977).
6. R. F. G. Gardner, F. Sweett and D. W. Tanner, J. Phys. Chem. Solids, 24, 1175 (1963); ibid, 24, 1183 (1963).

7. J. A. Crawford and R. W. Vest, J. Appl. Phys., 35, 2413 (1964).

8. L. J. van der Pauw, Phillips Research Rpts., 13, 9 (1958).

9. S. P. Tandon and J. P. Gupta, Spectrosc. Lett., 3, 297 (1970).

10. A. J. M. Kuipers and V. A. M. Brabers, Phys. Rev., B 14, 1401 (1976).

11. U. Buchenau and I. Müller, Solid State Comm., 11, 1291 (1972).

12. O. N. Salmon, J. Phys. Chem., 65, 550 (1961).

13. W. T. Read, Jr., Dislocations in Crystals, McGraw-Hill, New York (1953).

TABLE I

PREPARATION AND ANALYSIS OF n-TYPE Fe_2O_3

Authors (Reference #)	Sample Preparation	Structural and/or Compositional Analysis	ρ(300°K)	E_g (300°K)
Hardee & Bard (1)	Chemical vapor deposition (CVD) on Ti and Pt foils followed by firing to white-hot in Meeker burner flame for 1 min.	Polycrystalline from visual observation	"very low"	∿ 2.14 eV from photocurrent onset
Quinn, et al. (2)	Single crystals from PbF_2/PbO flux growth.	Single crystal α-Fe_2O_3 from x-ray diffraction	500 Ω cm	∿2.2 eV from photocurrent onset
Hardee & Bard (3)	CVD on Pt foil	Polycrystalline from CVD and salt evaporation. X-ray diffraction and SEM imply α-Fe_2O_3 with 20% ζ-Fe_2O_3, 10% Υ-Fe_2O_3	Not Reported	∿2.2 eV from photocurrent onset
	Evaporation of Fe_2O_3 salts			
	Natural Hematite	None		
Yeh & Hackerman (4)	Zone refined and magnetic iron and cold rolled steel heated red hot in air with Fisher burner for 15 min.	Polycrystalline from visual observation	Not Reported	∿ 1.4 eV from photocurrent onset
Kung, et al. (5)	Hydrothermal growth of crystals with 8M NaOH	Optical spectra suggests α-Fe_2O_3	< 10Ω cm	2.16 eV from optical density
This study	Chemical vapor transport using $TeCl_4$ as transport agent - Fe_2O_3 & $Fe_{2-x}Cr_xO_3$	X-ray diffractometer implies single phase α-Fe_2O_3 Cr content from neutron activation analysis	> 10^6 Ω cm	2.16 ± 0.03 eV from optical density

TABLE II

CONDITIONS FOR SUCCESSFUL GROWTH AND CHROMIUM ANALYSIS OF THE $Fe_{2-x}Cr_xO_3$ SINGLE CRYSTALS

Nominal Composition	Back-Transport Time (hrs) †	Transport Time (hrs)	Transport Temperature Gradient (°C)	Analysis ††
Fe_2O_3	18	222	1000/900	α-Fe_2O_3
$Fe_{1.90}Cr_{0.10}O_3$	23	144	1075/900	$Fe_{1.91}Cr_{0.09}O_3$
$Fe_{1.80}Cr_{0.20}O_3$	23	144	1075/900	$Fe_{1.78}Cr_{0.22}O_3$
$FeCrO_3$	24	130	1000/900	$Fe_{1.79}Cr_{0.21}O_3$
$FeCrO_3$	23	238	1000/900	$Fe_{1.53}Cr_{0.47}O_3$

† In all cases the back-transport temperature gradient was 900/450°C.

†† Analysis of the pure Fe_2O_3 sample was done by x-ray diffractometry. Chromium analysis was done by neutron activation analysis of the Cr^{51} (γ=321 keV) peak.

TABLE III

RESISTIVITIES (300°K) OF THE REDUCED Fe_2O_3 SAMPLES

a) Unpolished Samples

Sample# †	Reduction Temperature (°C)	Reduction Time (hrs)	d(cm)	ρ(Ω-cm)	ρ/d(Ω)
1A	350	163	.0020	1.7	850
1B	350	163	.0046	3.7	800
2	375	320	.0074	8.4	1150
3A	375	168	.0030	3.1	1050
3B	375	168	.0061	6.1	1000
3C	375	168	.0097	8.0	800
3D	375	168	.0150	16.4	1100
3E	375	168	.0221	25.5	1150
4	400	160	.0039	5.8	1500
5	400	167	.0091	10.0	1100

b) Polished Samples

Sample #	Reduction Temperature (°C)	Reduction Time (hrs)	d(cm)	ρ(Ω-cm)	ρ/d(Ω)
1C	350	163	.0084	2.2×10^4	2.6×10^6
3B	375	168	.0060	53.0	8850
3C	375	168	.0097	10.2	1050
3E	375	168	.0210	97.0	4600

† Samples having the same number, i.e. 1A, 1B, 1C were reduced in the same tube.

FIGURE CAPTION SHEET

FIG. 1 - X-ray powder diffraction patterns of α-Fe_2O_3 and Fe_3O_4. Note the appearance of Fe_3O_4 lines in the sample of α-Fe_2O_3 reduced at 350°C.

FIG. 2 - The room temperature optical density of a 0.0015(5) cm thick platelet of α-Fe_2O_3 showing the crystal field transitions at 1.44(3) and 2.16(3) eV.

FIG. 3 - The room temperature, unpolarized reflectivity of the c-face of an α-Fe_2O_3 crystal in the ultraviolet region of the spectrum.

FIG. 4 - Light and dark currents vs applied bias for a defect-free α-Fe_2O_3 platelet reduced at 350°C for 163 hrs (before sanding), in oxygen-free 0.2 M sodium acetate with the cathode at -0.65 volts vs SCE.

FIG. 5 - Photocurrents vs applied bias for a defect crystal of α-Fe_2O_3 reduced at 350°C for 218 hrs, in oxygen-free 0.2 M sodium acetate with the cathode at -0.64 volts vs SCE. The initial behavior and that after successive stages of sanding are shown in curves 1-4, respectively. The corresponding values for the ratios of light to dark currents at 1.5 V bias are given with the plotting symbols.

FIG. 6 - The dependence of the optical band gap of $Fe_{2-x}Cr_xO_3$ vs chromium content (x), at room temperature.

FIG. 7 - The room temperature optical densities of α-Fe_2O_3 (solid curve) and $Fe_{1.53}Cr_{0.47}O_3$ (dashed curve) showing the shift in the crystal field splitting of the 3d levels with chromium substitution.

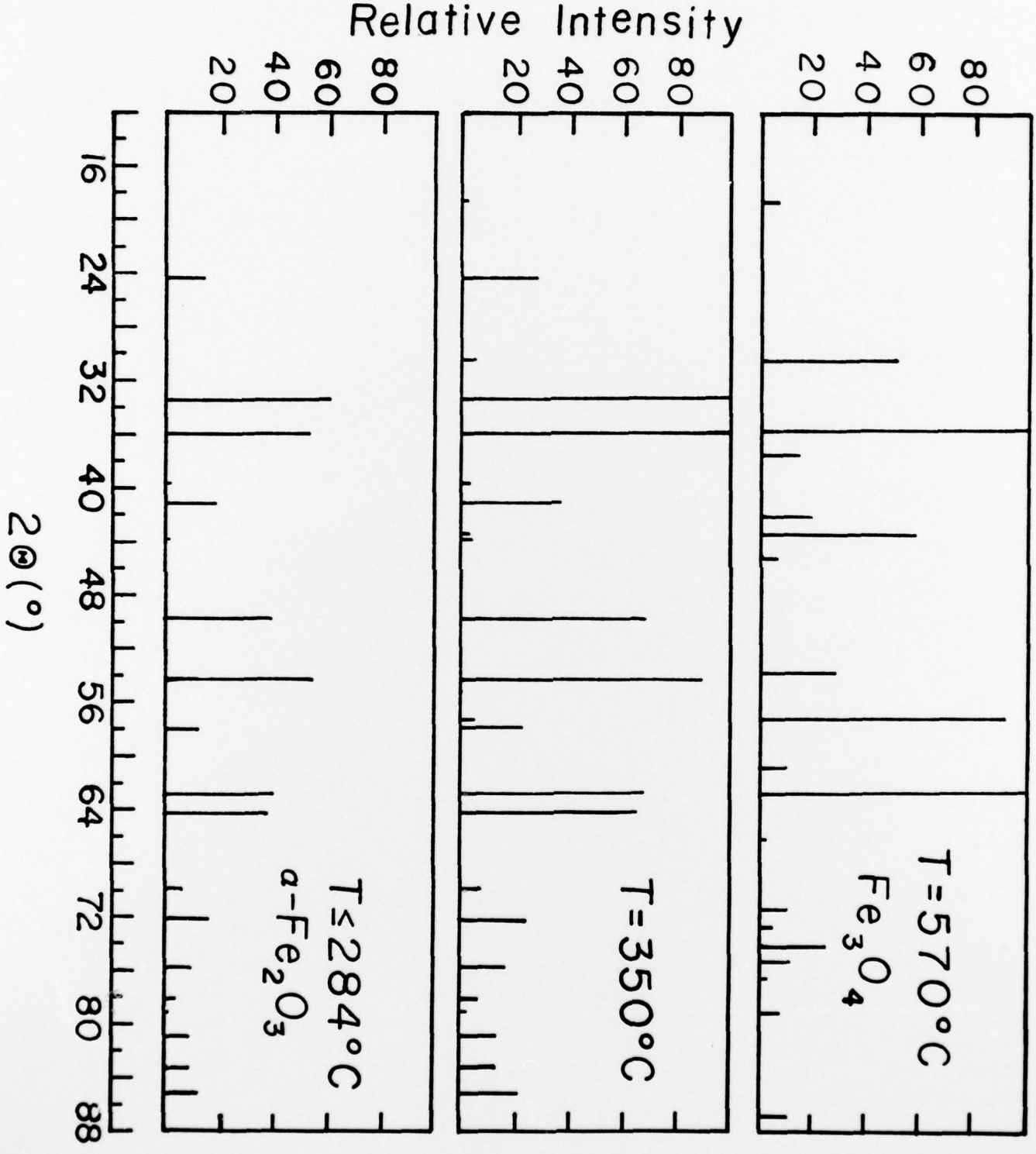
Relative Intensity
20
40
60
80
T=570°C
Fe_3O_4
T=350°C
T≤284°C
α-Fe_2O_3
16
24
32
40
48
56
64
72
80
88
2Θ(°)

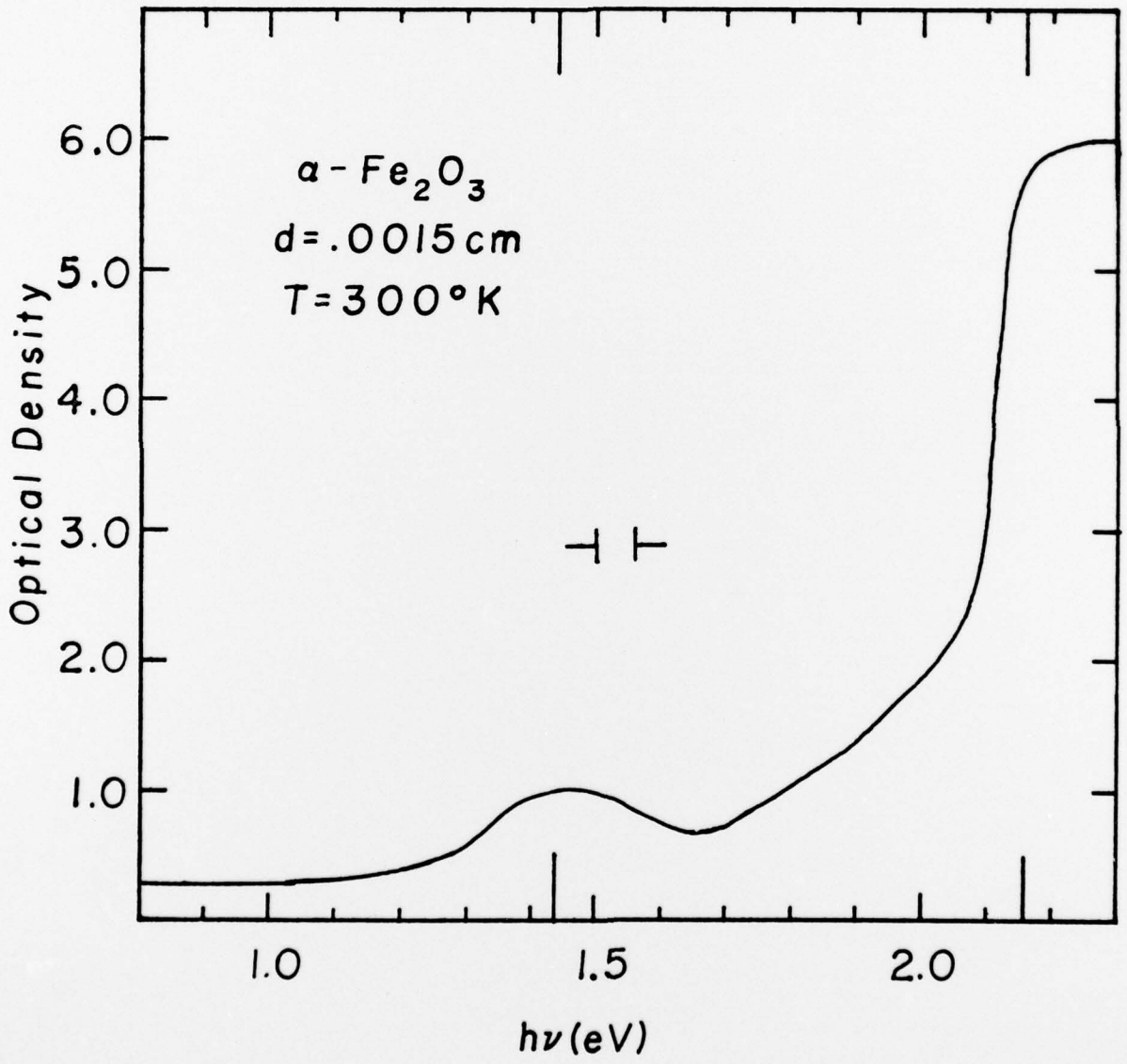
α - Fe2O3
d = .0015 cm
T = 300°K
Optical Density
6.0
5.0
4.0
3.0
2.0
1.0
1.0
1.5
2.0
hν (eV)

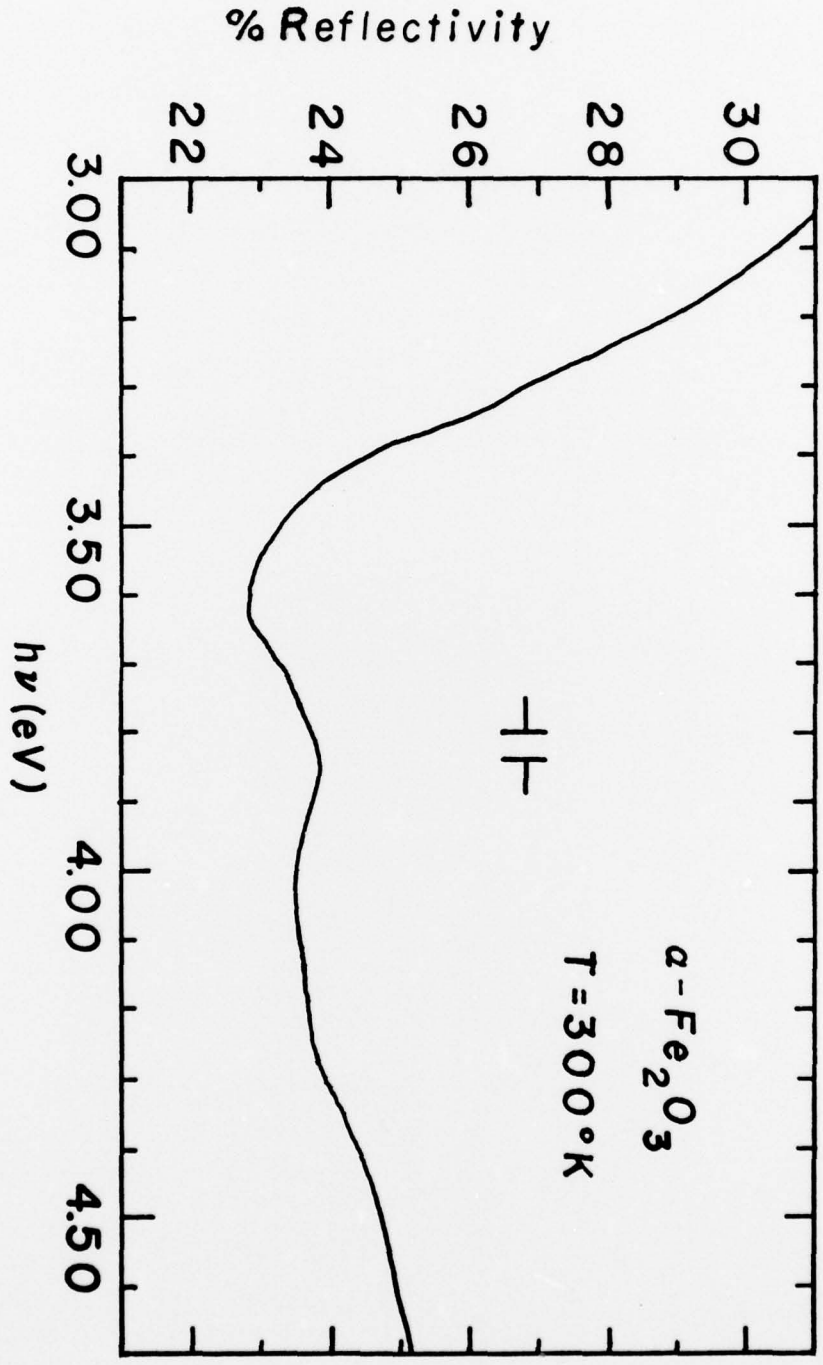
% Reflectivity
22
24
26
28
30
3.00
3.50
4.00
4.50
hν (eV)
α-Fe2O3
T=300°K

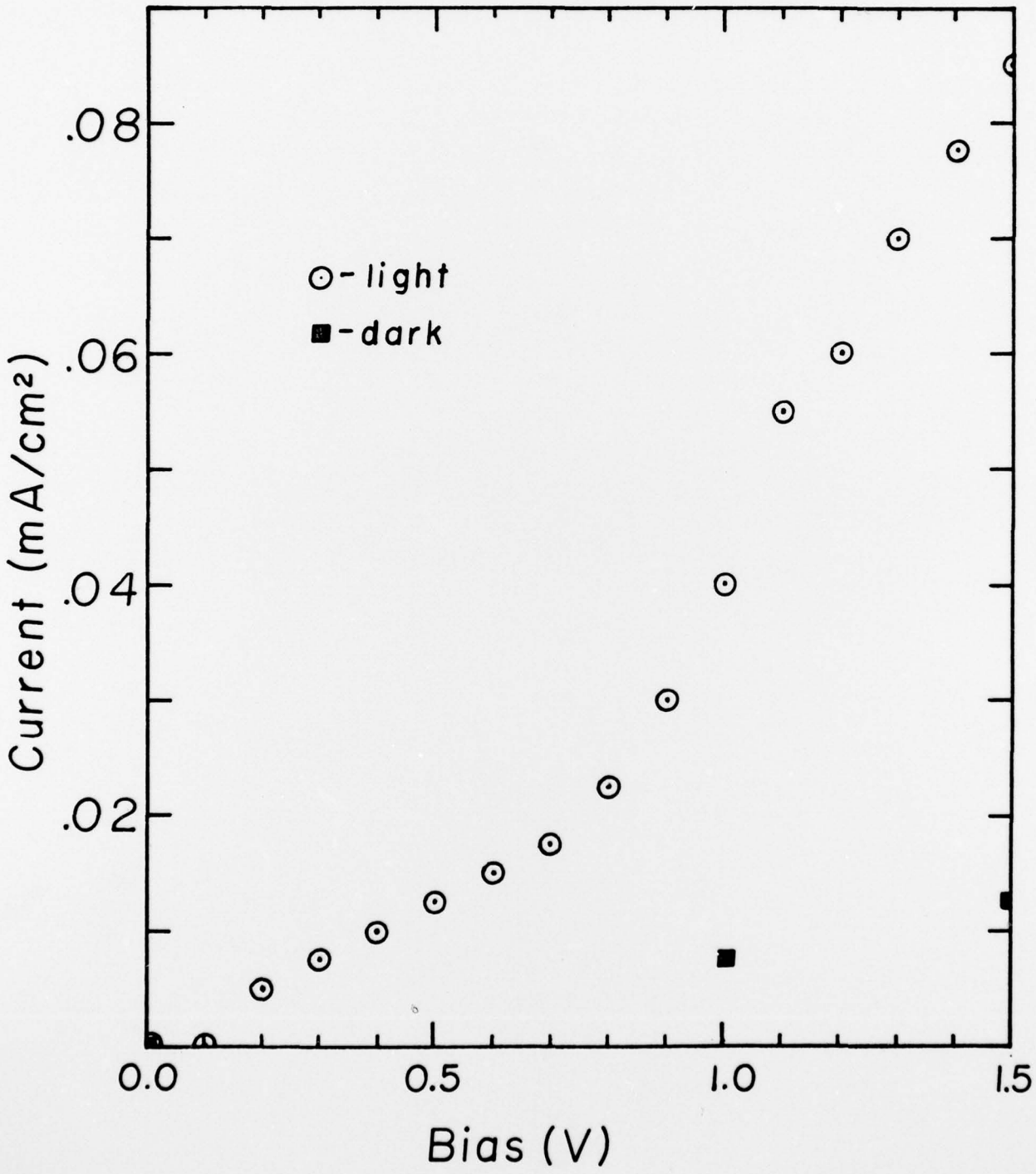
.08
.06
.04
.02
Current (mA/cm²)
⊙- light
■- dark
0.0
0.5
1.0
1.5
Bias (V)

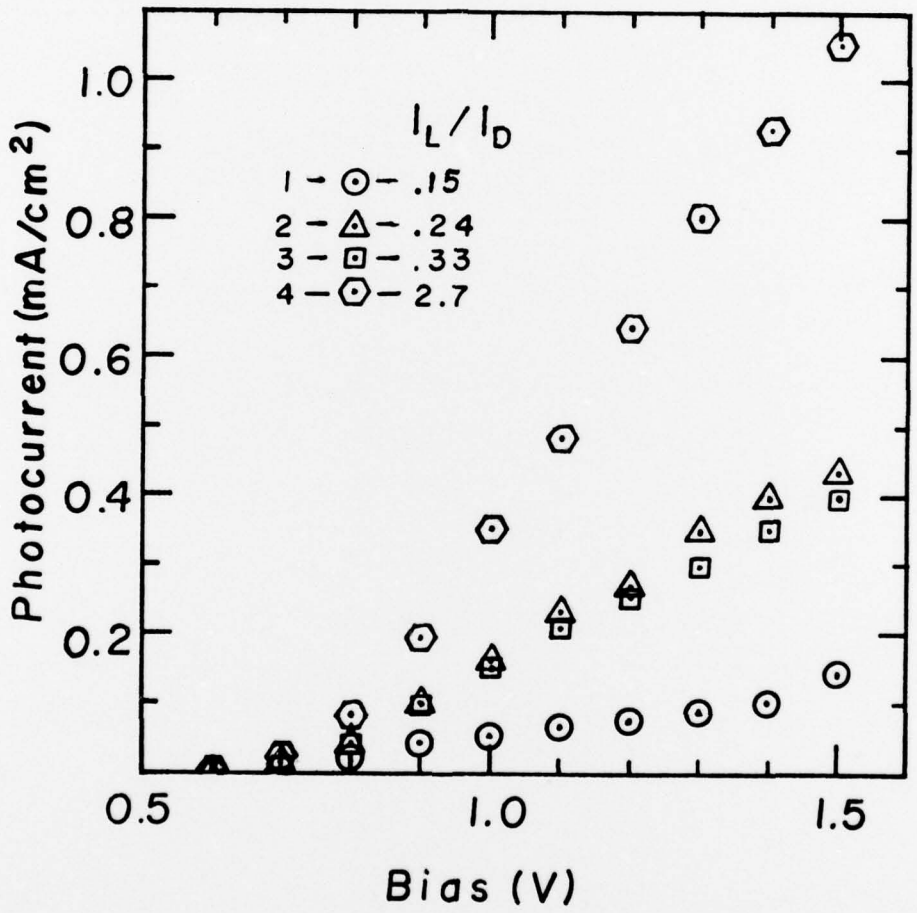
Photocurrent (mA/cm²)
1.0
0.8
0.6
0.4
0.2
0.5
1.0
1.5
Bias (V)
I_L / I_D
1 - .15
2 - .24
3 - .33
4 - 2.7

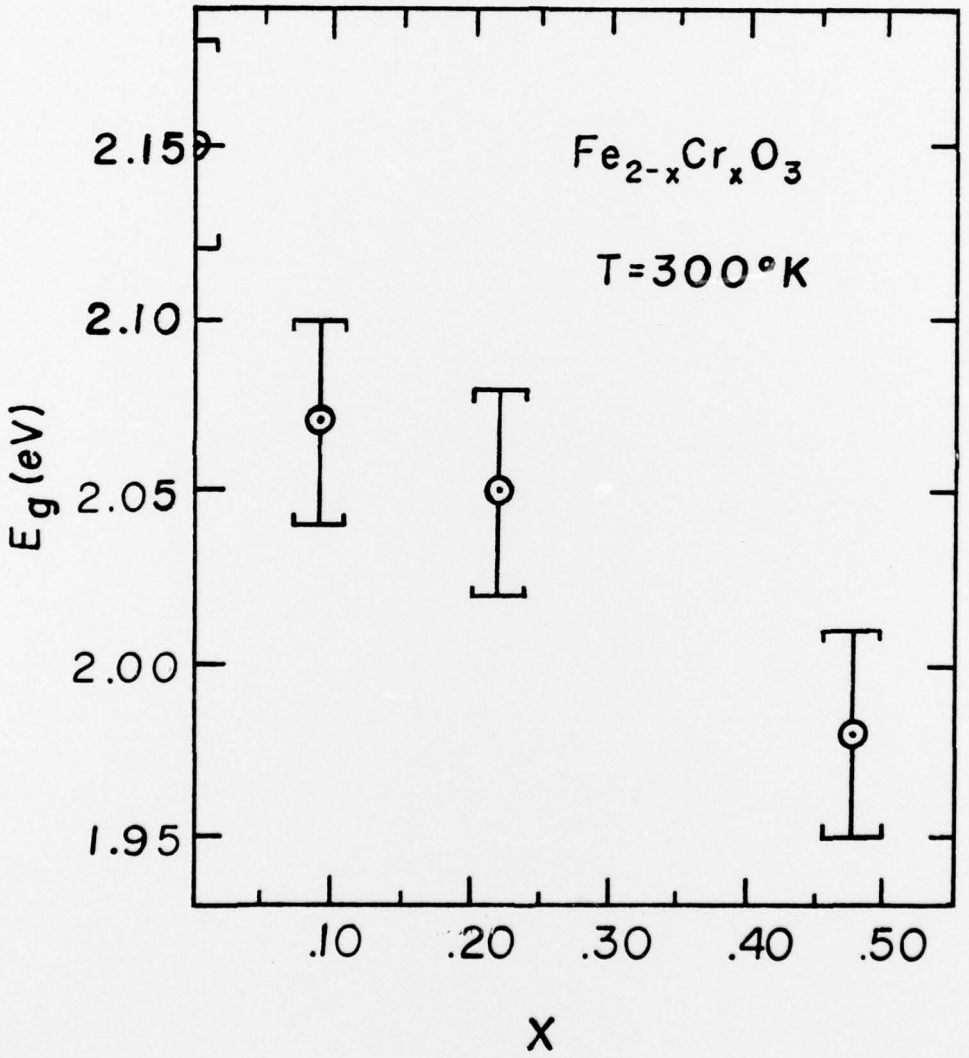
$Fe_{2-x}Cr_xO_3$
T=300°K
2.15
2.10
2.05
2.00
1.95
E_g (eV)
.10
.20
.30
.40
.50
X

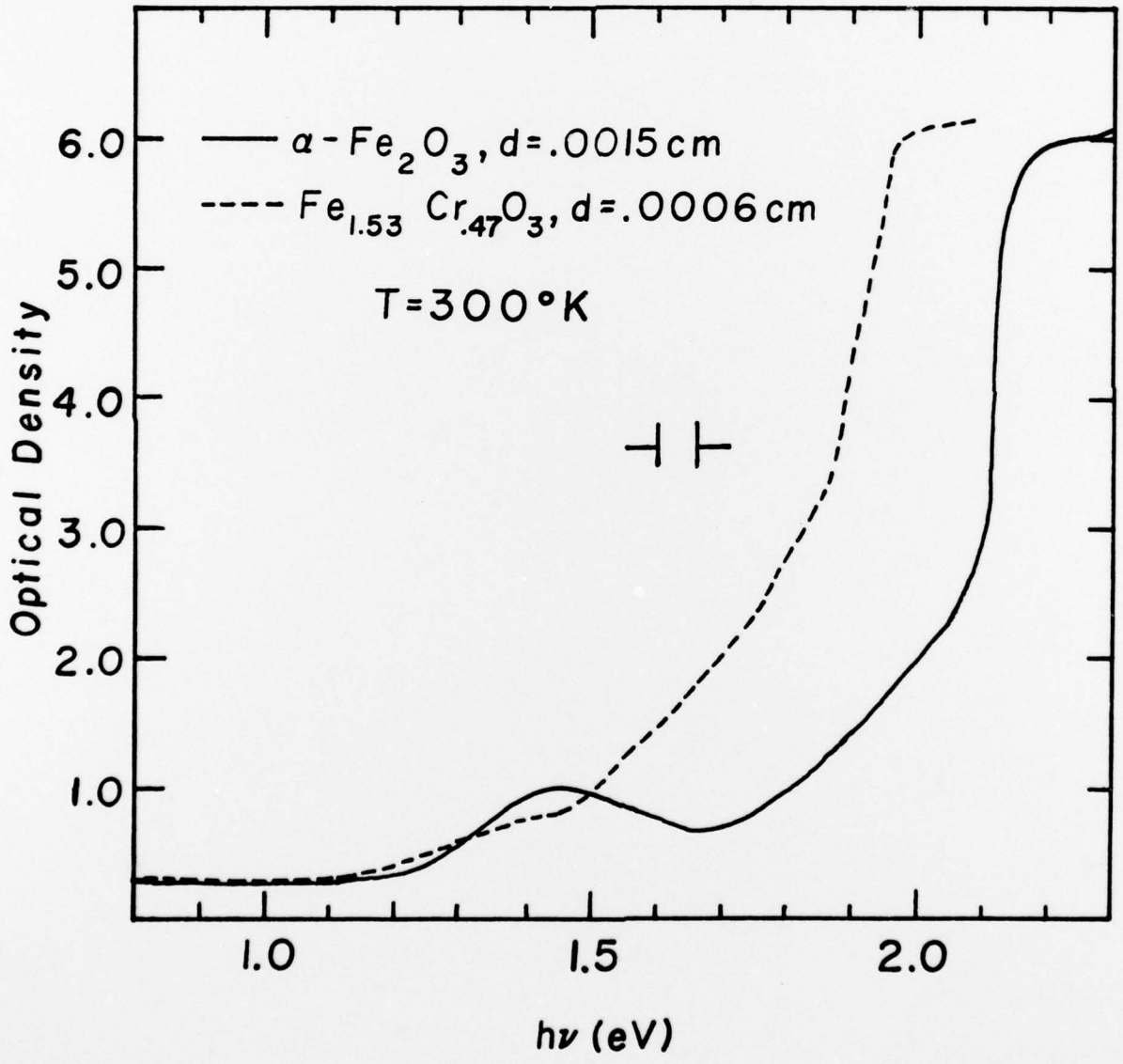
α - Fe2O3, d=.0015cm
Fe1.53 Cr.47O3, d=.0006cm
T=300°K
Optical Density
6.0
5.0
4.0
3.0
2.0
1.0
1.0
1.5
2.0
hν (eV)

Fig 1

FUTURE RESEARCH

During the second year of this program considerable effort will be made in attempting to prepare other oxyfluoride electrodes; specifically the system $SrTiO_{3-x}F_x$ will be studied. It is hoped that, because electrodes prepared from $SrTiO_3$ crystals show photocurrents at zero bias, we will be able to further improve the output by small substitutions of fluorine for oxygen. In addition, systems in which we substitute a +4 ion into the Fe_2O_3 structure will be studied. There has been to date no careful analysis of the nature of the photocurrents produced in the solid solution between Fe_2O_3 and $FeTiO_3$. This work will be extended to certain spinels--for example, $ZnFe_2O_4$- Fe_3O_4. The search for improved electrodes will be continued and studies will be started on possible p-type cathodes.

TECHNICAL REPORT DISTRIBUTION LIST

	No. Copies
Office of Naval Research Arlington, Virginia 22217 Attn: Code 472	2
Office of Naval Research Arlington, Virginia 22217 Attn: Code 102IP 1	6
ONR Branch Office 536 S. Clark Street Chicago, Illinois 60605 Attn: Dr. Jerry Smith	1
ONR Branch Office 715 Broadway New York, New York 10003 Attn: Scientific Dept.	1
ONR Branch Office 1030 East Green Street Pasadena, California 91106 Attn: Dr. R. J. Marcus	1
ONR Branch Office 760 Market Street, Rm. 447 San Francisco, California 94102 Attn: Dr. P. A. Miller	1
ONR Branch Office 495 Summer Street Boston, Massachusetts 02210 Attn: Dr. L. H. Peebles	1
Director, Naval Research Laboratory Washington, D.C. 20390 Attn: Code 6100	1
The Asst. Secretary of the Navy (R&D) Department of the Navy Room 4E736, Pentagon Washington, D.C. 20350	1
Commander, Naval Air Systems Command Department of the Navy Washington, D.C. 20360 Attn: Code 310C (H. Rosenwasser)	1
Defense Documentation Center Building 5, Cameron Station Alexandria, Virginia 22314	12
U.S. Army Research Office P.O. Box 12211 Research Triangle Park, N.C. 27709 Attn: CRD-AA-IP	1
Naval Ocean Systems Center San Diego, California 92152 Attn: Mr. Joe McCartney	1
Naval Weapons Center China Lake, California 93555 Attn: Head, Chemistry Division	1
Naval Civil Engineering Laboratory Port Hueneme, California 93041 Attn: Mr. W. S. Haynes	1
Professor O. Heinz Department of Physics & Chemistry Naval Postgraduate School Monterey, California 93940	1
Dr. A. L. Slafkosky Scientific Advisor Commandant of the Marine Corps (Code RD-1) Washington, D.C. 20380	1
Office of Naval Research Arlington, Virginia 22217 Attn: Dr. Richard S. Miller	1

TECHNICAL REPORT DISTRIBUTION LIST

	No. Copies
Dr. Paul Delahay New York University Department of Chemistry New York, New York 10003	1
Dr. R. A. Osteryoung Colorado State University Department of Chemistry Fort Collins, Colorado 80521	1
Dr. E. Yeager Case Western Reserve University Department of Chemistry Cleveland, Ohio 41106	
Dr. D. N. Bennion University of California Energy Kinetics Department Los Angeles, California 90024	1
Dr. R. A. Marcus University of Illinois Department of Chemistry Urbana, Illinois 61801	1
Dr. J. J. Auborn Bell Laboratories Murray Hill, New Jersey 07974	1
Dr. Adam Heller Bell Telephone Laboratories Murray Hill, New Jersey 07974	1
Dr. T. Katan Lockheed Missiles & Space Co., Inc. P.O. Box 504 Sunnyvale, California 94088	1
Dr. Joseph Singer, Code 302-1 NASA-Lewis 21000 Brookpark Road Cleveland, Ohio 44135	1
Dr. S. B. Brummer EIC Corporation 55 Chapel Street Newton, Massachusetts 02158	1
Mr. Frank Murphy GTE Laboratories 40 Sylvan Road Waltham, Massachusetts 02154	1

	No. Copies
Library P. R. Mallory and Company, Inc. P.O. Box 706 Indianapolis, Indiana 46206	1
Dr. P. J. Hendra University of Southampton Department of Chemistry Southampton SO9 5NH United Kingdom	1
Dr. Sam Perone Purdue University Department of Chemistry West Lafayette, Indiana 47907	1
Dr. Royce W. Murray University of North Carolina Department of Chemistry Chapel Hill, North Carolina 27514	1
Naval Ocean Systems Center San Diego, California 92152 Attn: Technical Library	1
Dr. J. H. Ambrus The Electrochemistry Branch Materials Division, Research & Tech. Dep Naval Surface Weapons Center White Oak Laboratory Silver Spring, Maryland 20910	1
Dr. G. Goodman Globe-Union Inc. 5757 North Green Bay Avenue Milwaukee, Wisconsin 53201	1
Dr. J. Boechler Electrochimica Corporation Attention: Technical Library 2485 Charleston Road Mountain View, California 94040	1
Dr. P. P. Schmidt Oakland University Department of Chemistry Rochester, Michigan 48063	1

TECHNICAL REPORT DISTRIBUTION LIST

	No. Copies
~~Dr. Aaron Wold~~ ~~Brown University~~ ~~Department of Chemistry~~ ~~Providence, Rhode Island 02912~~	1
Dr. R. C. Chudacek McGraw-Edison Company Edison Battery Division Post Office Box 28 Bloomfield, New Jersey 07003	1
Reliability Analysis Center ATTN: I. L. Krulac Griffiss AFB, N.Y. 13441	1

	No.
Mr. D. L. Warburton The Electrochemistry Branch Materials Division, Research & Te Dept. Naval Surface Weapons Center White Oak Laboratory Silver Spring, Maryland 20910	